SANDIA REPORT SAND84—0237 • Unlimited Release • UC—62
Printed October 1984

Total Normal Emittance Measurements of Highly Conductive, Opaque Materials Using a Solar Furnace

Billy W. Marshall, Jr., George P. Mulholland, Robert M. Edgar

Prepared by
Sandia National Laboratories
Albuquerque, New Mexico 87185 and Livermore, California 94550
for the United States Department of Energy
under Contract DE-AC04-76DP00789

Issued by Sandia National Laboratories, operated for the United States Department of Energy by Sandia Corporation.

Printed in the United States of America
Available from
National Technical Information Service
U.S. Department of Commerce
5285 Port Royal Road
Springfield, VA 22161

NTIS price codes
Printed copy: A03
Microfiche copy: A01

SAND84-0237
Unlimited Distribution
UC-62
Printed October 1984

TOTAL NORMAL EMITTANCE MEASUREMENTS OF HIGHLY CONDUCTIVE, OPAQUE MATERIALS USING A SOLAR FURNACE

Billy W. Marshall, Jr.
Severe Accident Containment Response Division 6427

George P. Mulholland
New Mexico State University

Robert M. Edgar
Solar Thermal Test Facility Division 6222

ABSTRACT

This report presents a method for measuring the total normal emittance of a conductive opaque material with and without a selective surface coating and at elevated temperatures. The purpose was to develop a method for measuring surface properties of materials subjected to highly concentrated solar flux. A horizontal axis solar furnace was used to heat the samples to temperatures ranging from 373 to 973 K (100° to 700°C), with all tests conducted in air. A Kendell MK-VI radiometer consisting of a cavity-type radiometer and a control unit was used to measure the total normal emittance. The emittance measurements for both copper and aluminum at 373 and 473 K (100° and 200°C) were found to be unreliable because of relatively high drift in the cavity-type radiometer system compared to the emitted energy at these temperatures. However, total normal emittance measurements of these materials at 573 K (300°C) and above compare favorably with trends of published data. A Kline-McClintock uncertainty analysis was performed with experimental uncertainties of ±10% to 15% of the emittance value obtained.

ACKNOWLEDGMENTS

Dr. Richard Pettit and Mr. John Holmes of Sandia National Laboratories were instrumental in the design, implementation, and evaluation of this experimental procedure.

The authors also wish to express their sincere appreciation to the personnel at the Central Receiver Test Facility at Sandia National Laboratories, especially Mr. John Otts and Mr. John Holmes, for their time and efforts while conducting the experiment. Thanks to Dr. Richard Pettit of the Thermophysical Properties Division of Sandia National Laboratories for providing literature and advice about the experimental techniques used to measure radiative properties.

In addition, Dr. Pettit and Mr. Rod Mahoney measured the total normal emittance of each sample at 373 K (100°C) in their laboratory throughout the course of this experimental work.

Melissa Watkins and the personnel from Tech. Reps., Inc., were most helpful in putting this text together. To these and others not mentioned here, we extend our sincere appreciation.

CONTENTS

		Page
1.	INTRODUCTION	1
2.	BACKGROUND	7
	2.1 Radiative Properties	7
	2.2 Blackbody Emitters	7
	2.3 Real Surface Emitters	9
	2.4 Blackbody Sources	11
3.	EXPERIMENTAL DESIGN	13
	3.1 Objectives	13
	3.2 Assumptions	15
	3.3 Description of the Solar Furnace	18
	3.4 Experimental Apparatus	19
	3.5 Experimental Uncertainty	22
4.	EXPERIMENTAL PROCEDURES	25
	4.1 Sample Preparation	25
	4.2 Temperature Gradient Measurements	26
	4.3 Blackbody Calibration	26
	4.4 Emittance Measurements	27
	4.5 Flux Field Map	30
5.	RESULTS AND DISCUSSION	33
	5.1 Temperature Difference Measurements	33
	5.2 Flux Field Map	33
	5.3 Total Normal Emittance Measurements	36
6.	CONCLUSIONS	45
7.	RECOMMENDATIONS	47
APPENDIXES		
	A Total Normal Emittance Data at 373 K (100°C)	49
	B Conduction and Convection Losses	51
	C Solution to Temperature Distribution	55
REFERENCES		57

ILLUSTRATIONS

Figure		Page
1	Directional Dependence of Intensity from an Elemental Surface Area dA	10
2	Blackbody Source Geometry	12
3	Experimental Setup	14
4	CRTF Solar Furnace	20
5	Thermocouple Placement	26
6	Blackbody Calibration Curve	28
7	Three-Dimensional Flux Plot of the Incoming Flux Field	34
8	Isoflux Plot with the Sample Superimposed	35
9	Total Normal Emittance of Aluminum	37
10	Total Normal Emittance of Copper	39
11	Touloukian Total Normal Emittance of Aluminum	40
12	Touloukian Total Normal Emittance of Copper	40
13	Analyzed Total Normal Emittance of Copper	41
14	Total Normal Emittance of Pyromark Coatings	43

TABLES

Table		Page
1	Smallest Real Root of the Polynomial $A^4 + K_1A^3 + K_2A^2 + K_3A + K_4 = 0$	17
2	Temperature Difference from the Front to the Back Surface	18
3	Kendell MK-VI System Specifications	22
4	Measured Temperature Difference from Central Thermocouple (#9) on the Front Surface	34

NOMENCLATURE

A_n = Area normal to the radiation field, cm^2

A_t = Total surface area that convects and emits energy, cm^2

c = Thermal conductance of the 3000 Board, $W/(cm^2\ °C)$

C_1 = First radiation constant = 5954.4 $W/(\mu m^4\ cm^2)$

C_2 = Second radiation constant = 14388 $\mu m\ K$

C = Specific heat of the sample, J/(kg °C)

C_p = Specific heat of the convecting fluid at constant pressure, J/(kg °C)

C.F. = Calibration factor for the reference flux reading, $W_{thermal}/(watt/cm^2)$

d = Abscissa scale factor, dimensionless

$e_b(T)$ = Total hemispherical emissive power of a blackbody, $W/(cm^2\ \mu m)$

$e_b(\lambda,T)$ = Hemispherical spectral radiant intensity of a blackbody, $W/(cm^2\ \mu m)$

$e(\lambda,\theta,T)$ = Directional spectral emissive power of a real surface, $W/(cm^2\ \mu m)$

$e(\theta,\phi,T)$ = Directional total emissive power of a real surface, $W/(cm^2\ \mu m)$

$e(\lambda,\theta,\phi,T)$ = Directional spectral emissive power of a real surface, $W/(cm^2\ \mu m)$

g = Local acceleration of gravity, cm/s^2

h(T) = Average film coefficient over a plate length L, $W/(cm^2\ °C)$

$h_x(T)$ = Local heat transfer coefficient, $W/(cm^2\ °C)$

$i_b(T)$ = Total hemispherical radiant intensity of a blackbody, $W/(cm^2\ \mu m\ rad)$

$i_b(\lambda,T)$ = Hemispherical spectral radiant intensity of a blackbody, $W/(cm^2\ \mu m\ rad)$

k = Thermal conductivity of the convecting fluid, W/(cm °C)

K = Thermal conductivity of the sample material, W/(cm °C)

L = Length of the plate, cm

m = Mass of the sample, kg

N_{gr} = Grashoff Number, dimensionless

N_{pr} = Prandtl Number, dimensionless

Power = Probability that a test will yield accurate results, dimensionless

q = Incoming radiation flux striking the sample, W/cm^2

q_r = Radial heat flow from the sample to the 3000 Board, W

Q_a = Absorbed energy, W

Q_i = Incident energy, W

Q_{in} = Energy absorbed by the sample, W

Q_{out} = Energy leaving the sample, W

Q_r = Reflected energy, W

Q_t = Transmitted energy, W

r_i = Radius of the sample, cm

r_o = Radius from the center of the sample to the outer edge of the 3000 Board, cm

t = Thickness of the sample, cm

T = Absolute steady-state temperature, K

$T(x)$ = Temperature as a function of the material thickness, K (°C)

$\bar{T}$ = Average temperature of the convecting fluid, K (°C)
= $1/2(T + T_\infty)$

T_∞ = Temperature of the convecting fluid far removed from the plate, K (°C)

T_h = Temperature of the front surface of the sample, K (°C)

T_i = Temperature of the sample, °C

T_o = Temperature at the outer edge of the 3000 Board, °C

T_{sc} = Surrounding temperature for convection, K (°C)

T_{sr} = Surrounding temperature for radiation, K (°C)

w_{e_n} = Uncertainty of the normal real surface emittance measurement

$w_{e_{bn}}$ = Uncertainty of the normal blackbody emittance measurement

Greek Symbols

α' = Probability of a Type I error occuring, dimensionless

α = Coefficient of volume expansion, K^{-1}

β' = Probability of a Type II error occuring, dimensionless

$\varepsilon(T)$ = Total hemispherical emittance at temperature T, dimensionless

$\varepsilon_n(T)$ = Total normal emittance of a real surface, dimensionless

$\varepsilon(\theta,\phi,T)$ = Directional total emittance of a real surface, dimensionless

$\varepsilon(\lambda,\theta,\phi,T)$ = Directional spectral emittance of a surface, dimensionless

ℓ = Calculated thickness of the sample, cm

λ = Wavelength of the radiation, μm

μ = True mean value of the set of data points

μ^* = Dynamic viscosity of the convecting fluid, kg(cm s)

μ_o = Actual mean value of a set of data points

ν = Kinematic viscosity of the fluid, cm^2/s

π = 3.1415927

ρ_f = Density of the convecting fluid, kg/cm^3

σ = Stefan-Boltzmann constant

= 5.729×10^{-12} $W/(cm^2\ K^4)$

σ^* = Standard deviation of a set of data points

θ = Angle at which the energy is measured with respect to the surface normal

TOTAL NORMAL EMITTANCE MEASUREMENTS OF HIGHLY CONDUCTIVE, OPAQUE MATERIALS USING A SOLAR FURNACE

1. INTRODUCTION

At temperatures above absolute zero, all matter is continually emitting energy by radiation as a result of thermal vibrations of the material particles (electrons, ions, etc.). The emittance of a surface is a measure of how well the surface emits radiation as compared to an ideal "black" surface. The thermal radiative properties of pure, optically smooth surfaces generally depend upon wavelength, angular direction, and temperature of that surface. Real surface properties additionally depend upon surface roughness, surface films, surface preparation, thermal history, and environmental interaction. Oxide films in particular may affect the radiative properties of a material and change the radiative characteristics with thickness.

Many experimental techniques for measuring the emittance, and more generally the thermal radiative properties, of opaque surfaces have been described in the literature. These methods fall into two general categories, calorimetric and radiometric.[1] In calorimetric techniques, the energy absorbed or emitted by a sample is evaluated in terms of the energy lost or gained by the sample. In radiometric techniques, the emitted or reflected energy is measured directly.

Calorimetric techniques are most generally used to measure the absorptance and emittance of a surface. This technique is not suitable for reflectance measurements. Generally, a

sample is placed in a vacuum such that all of the heat transfer to or from the sample is by radiation only. The sample is electrically heated and the power input to the heater accurately measured. When a steady-state condition is achieved, the power to the heater can be directly equated to the heat output of the sample. The desired properties can be computed when the steady-state temperature of the sample, the measured rate of radiant heat transfer (which is equal to the steady-state input of electrical power), the temperature of the surroundings and the geometry of the system are known.

In radiometric techniques, the radiant flux (emitted, incident, reflected, or any combination of these) is measured directly, and the desired property is computed as the approximate ratio of the measured fluxes. The thermal emittance of a sample may be measured directly by computing the ratio of the energy emitted by the sample to that of a blackbody source at the same temperature, geometric, and spectral conditions. The comparison blackbody may be either an integral blackbody cavity, whose walls are formed by the sample,[2] or a separate blackbody controlled at the temperature of the sample.[3,4] The separate blackbody technique is most accurate at temperatures below 1800 K (1527°C), where temperature measurements and control by use of thermocouples present no serious problems.

Richmond, Harrison, and Shorten developed a method to measure the normal spectral emittance by the radiometric technique.[5] A sample was heated by passing an electrical current through it, resulting in temperatures ranging from 800 to 1400 K (527° to 1127°C). The normal spectral emittances from 1 to 15 μm of three samples considered as laboratory standards for low, intermediate, and high emittance were also measured. The results for the sample agreed quite well with these laboratory standards and had an overall reproducibility of 0.005 emittance units.

Pettit and Sowell presented a method for evaluating the solar absorptance and total hemispherical emittance of solar selective coatings.[5,6] The total hemispherical emittance was determined by maintaining a sample at a steady-state temperature inside a blackened, liquid nitrogen-cooled vacuum chamber. The sample was heated to a steady-state temperature using an electrical heater. The electrical power supplied to the heater was then equated to the total hemispherical emittance using the Stephan-Boltzmann equation. The experimental errors were reported as being less than ± 0.045 emittance units or less for emittances between 0.3 and 1.0.

Moore employed the radiometric technique to measure the total normal emittance.[2] These measurements were made on small samples with shallow reference holes. The emittance was calculated using a theoretical expression relating the emittance to the ratio of the radiant flux density from the sample to that of the flux density within the shallow hole in the sample. The expression used applies only to diffusely reflecting materials. The results of the emittance measurements on four materials were determined to be in good agreement with values obtained by a heated strip method. However, systematic errors were discovered in the system and no firm conclusions about the accuracy of the measurements could be made.

Gravina, Bastian, and Dyer described the procedures and equipment used to measure simultaneously the spectral and total normal emittance over a temperature range from 473 to ~1273 K (200° to ~1000°C).[4] The apparatus consists of a vacuum system, a test chamber that is either evacuated or left at ambient conditions, a reference blackbody, and a single-beam, dual-channel radiometer that gives both total and spectral data simultaneously. A root mean square error analysis of the data was performed, reporting a ±8% error for the

vacuum test. The results of the measurements, both spectral and total, compared favorably to published normal emittance data.

Grammer and Streed developed a water-cooled evacuated chamber used to measure the total hemispherical and total directional and spectral emittance over the temperature range from 673 to 2273 K (400° to 2000°C).[7] The total and spectral emittances were determined by comparing the emitted radiation from the surface to a reference blackbody enclosure in the same geometry and at the same temperature. Experimental uncertainties of less than 10% of the measured value were reported for a variety of samples.

Evans, Clayton, and Fries present a method to measure rapidly the total normal emittance of an opaque surface between 813 and 1923 K (540° and 1650°C) with all tests conducted in air.[8] The method uses a 10-kW search lamp that collimates the energy to a concentrator. This energy is then focused onto the back of a sample located at the focal plane of the concentrator. A Brown Instrument Company miniature radiometer was used to measure the energy emitted from the sample. The total normal emittance is calculated as the ratio of this measurement to that of a blackbody in the same geometry and at the same temperature. The accuracy of the measurement was published to be ±10% or less depending upon the instrument used to record the sample temperature (i.e., thermocouples or an optical pyrometer).

With the emergence of solar energy as a viable alternate energy, the performance of the collector, whether it be a flat-plate collector for residential applications or a collector used at high temperatures and concentrations of solar flux, is directly affected by the performance of the solar absorbing surface. Therefore, methods are needed to measure the thermal radiative properties of materials and coatings

being irradiated by the sun. In particular, a rapid method for estimating the radiative properties of materials used in collectors tested at Sandia's Central Receiver Test Facility would be very useful. A great deal of laboratory work and analytical modeling has been performed by Pettit to evaluate solar coatings such as black chrome.[5,6,9] It is the objective of this research to present a rapid, reliable method for evaluating the radiative properties. In particular, the total normal emittance of materials, with or without applied coatings, that are being directly irradiated by the sun will be considered.

The general methods of Evans, Clayton, and Fries, presented earlier, were used to heat samples to a uniform steady-state temperature in a horizontal axis solar furnace. The total normal emittance was then obtained from the ratio of the measured total normal emissive power of a surface to that of a reference blackbody. The samples were tested at atmospheric conditions since generally the surfaces are exposed to these conditions in actual solar applications. This approach to measuring radiative properties should be viewed as an in situ engineering approach rather than the more exact laboratory approach of many of the references already cited.

2. BACKGROUND

2.1 Radiative Properties

When a body is irradiated, part of the incident radiation is reflected, part is absorbed, and the remaining energy is transmitted. By conservation of energy, the sum of the absorbed energy Q_a, the reflected energy Q_r, and the transmitted energy Q_t, is equal to the incident energy Q_i:

$$Q_i = Q_a + Q_r + Q_t \ . \qquad (1)$$

Thermal radiative properties of a large class of materials are strongly influenced by surface effects due to surface preparation and finishing, thermal history, and environmental interaction. In particular, oxide films may significantly affect the thermal radiative properties of a surface. These oxide films may change in thickness and in radiative character as a result of (1) heating the material in the oxidizing atmosphere, (2) the length of time the heated material is exposed to the oxidizing atmosphere, and (3) the number of times the material has been heated from the ambient temperature to an elevated temperature. Therefore, by convention, the radiative properties will end in "ance" since they are not intrinsic properties of the material.

2.2 Blackbody Emitters

A blackbody radiator absorbs all the radiant energy incident upon it and emits the maximum possible amount of energy per unit area at any wavelength and in a given direction at a given temperature. When making experimental measurements of the emittance of a real surface, a blackbody

source is needed for a direct comparison between the real surface and the ideal "black" surface. Some important properties of ideal blackbody surfaces will now be discussed.

A blackbody emits energy hemispherically and spectrally such that the radiant intensity, $i_b(\lambda,T)$, is independent of direction. The hemispherical spectral emissive power, $e_b(\lambda,T)$, of a blackbody can be developed[10] in terms of the hemispherical spectral radiant intensity as

$$e_b(\lambda,T) = \pi i_b(\lambda,T) \ . \tag{2}$$

The spectral distribution of this hemispherical emissive power is given by Planck's equation,

$$e_b(\lambda,T) = \frac{2\pi C_1}{\lambda^5(\exp(C_2/\lambda T) - 1)} \tag{3}$$

where C_1 is the first radiation constant equal to 5954.4 $W/(\mu m4\ cm^2)$, C_2 is the second radiation constant equal to 14,388.0 $\mu m\ K$, λ is the wavelength in μm, and T is the absolute steady-state temperature. The medium into which the energy is emitted is assumed to have an index of refraction of 1.0 (air).

The hemispherical total radiant intensity emitted by a blackbody can be developed by integrating the hemispherical spectral intensity over all wavelengths. The results are well known as

$$i_b(T) = \frac{\sigma}{\pi} T^4 \tag{4A}$$

where

$$\sigma = \frac{2C_1\pi^5}{15C_2^4} . \tag{4B}$$

The hemispherical total emissive power of a blackbody is then

$$e_b(T) = \pi i_b(T) = \sigma T^4 , \tag{5}$$

which is the Stefan-Boltzmann law.

An additional property of an ideal black surface is that it emits energy directionally according to Lambert's cosine law. Generally stated, Lambert's law is

$$e_b(\lambda,\theta,T) = i_b(\lambda,T)\cos(\theta) \tag{6}$$

where $e_b(\lambda,\theta,T)$ is the directional spectral emissive power of a blackbody at a steady-state temperature T and angle θ as measured from the surface normal. Because a blackbody is a diffuse surface (i.e., it follows Lambert's law) at all temperatures, it serves as a standard for comparison with the directional properties of real surfaces that do not in general follow this cosine law.

2.3 Real Surface Emitters

The emittance of a surface is a measure of how well it can radiate energy compared with a blackbody. The emittance of a real surface is defined as the ratio of the emitted energy of that surface to that of a blackbody at the same temperature. This definition leads to the most general emittance equation

$$\varepsilon(\lambda,\theta,\phi,T) = \frac{e(\lambda,\theta,\phi,T)}{e_b(\lambda,\theta,T)} \tag{7}$$

because it includes the dependence on wavelength, direction, and surface temperature. Figure 1 illustrates the directional dependence of the radiant intensity leaving a surface.

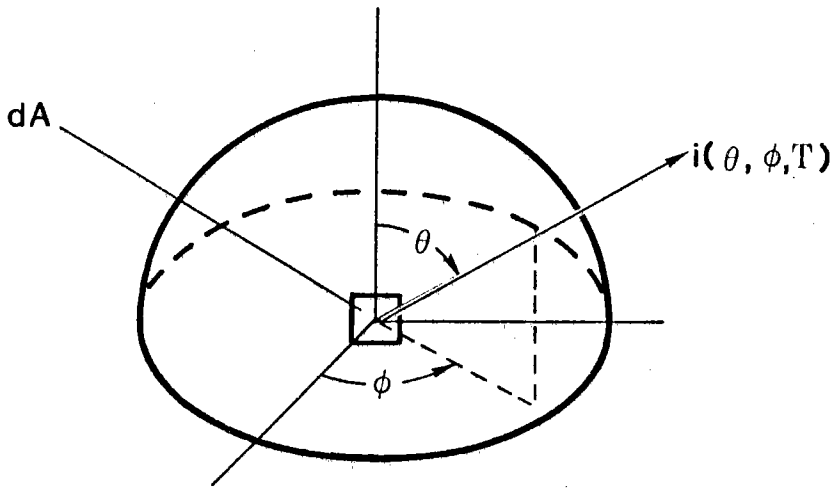

Figure 1. Directional Dependence of Intensity from an Elemental Surface Area dA

The directional total emissive power of a real surface is found by integrating the directional spectral emissive power of a surface over the entire spectrum, that is,

$$e(\theta,\phi,T) = \int_0^\infty e(\lambda,\theta,\phi,T)\, d\lambda \ . \qquad (8)$$

The directional total emittance of a real surface at some steady-state temperature, T, is the ratio of Eq. 8 to the integral of Eq. 7 over all wavelengths, and is given by

$$\varepsilon(\theta,\phi,T) = \frac{\pi}{\sigma T^4 \cos(\theta)} \int_0^\infty e(\lambda,\theta,\phi,T)\, d\lambda \qquad (9)$$

where

$$e_b(\theta,T) = \int_0^\infty \varepsilon_b(\lambda,\theta,T)d\lambda = \frac{\sigma T^4}{\pi} \cos\theta \ . \qquad (10)$$

The total normal emittance of a surface can now be defined for the case where $\theta = 0$ and $\phi = 0$, as

$$\varepsilon_n(T) = \frac{\pi}{\sigma T^4} \int_0^\infty e(\lambda,0,0,T)\ d\lambda \ . \qquad (11)$$

This equation implies that if the total normal emissive power of a real surface is measured experimentally, then the total normal emittance can be calculated. Additionally, if the total normal emissive power of a blackbody source is measured experimentally, then by Eq. 7, the ratio of the two measurements is the total normal emittance of the real surface.

2.4 Blackbody Sources

When making experimental measurements of the radiative properties of real surfaces using a radiative technique, it is desirable to have a blackbody source for reference so that direct comparisons can be made between the real surface and the ideal black surface. One often used, close approximation to a blackbody source, is a metal cylinder that has been hollowed out to form a cavity with a relatively small opening. If the opening is made sufficiently small compared to the cylinder diameter and length and the cylinder cavity walls are coated with a black, highly absorbing surface, then the opening area approaches the behavior of an ideal "black" surface because essentially all the radiation entering the opening is absorbed. By heating the cavity walls to a uniform steady-state temperature, a source of a blackbody radiation is obtained at the opening.

The blackbody source used as the comparison standard in this experiment is a commercial unit made by Barnes Engineering (Model #11-201T). This unit has a 28° solid angle, cone-shaped cavity as shown in Figure 2, with an effective aperture diameter of 2.54 cm, an effective aperture emissivity of 0.99 ± 0.01 and an operating temperature ranging from 473 to 1273 K (200° to 1000°C).[11]

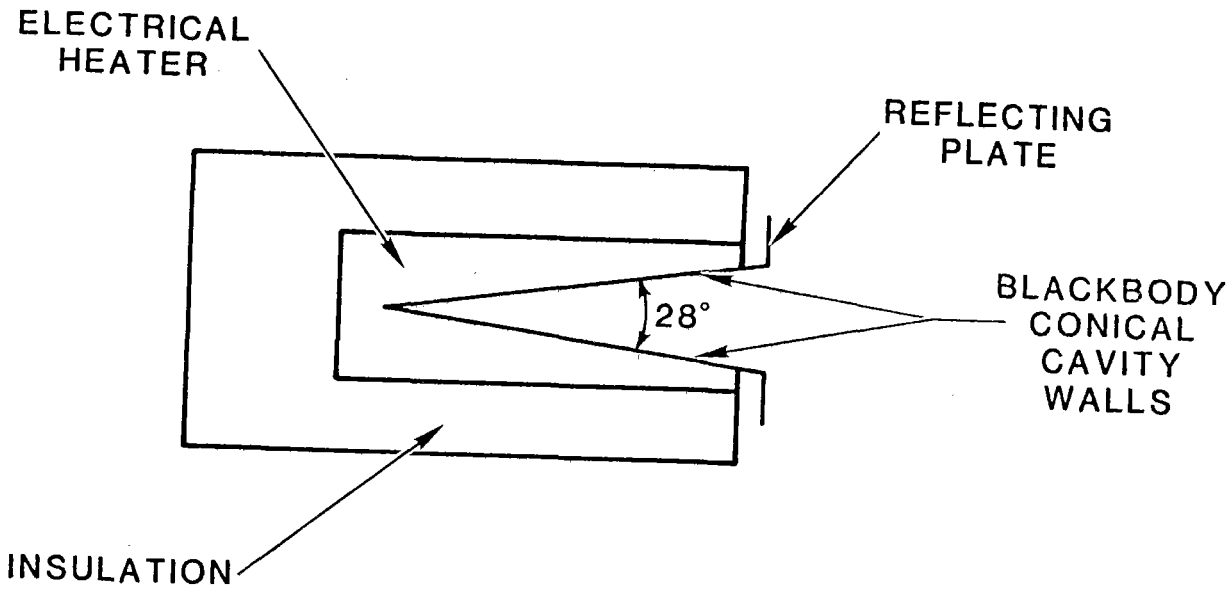

Figure 2. Blackbody Source Geometry

3. EXPERIMENTAL DESIGN

3.1 Objectives

In accordance with the primary objective of developing an experimental-type technique, some sacrifices in experimental accuracy have been made to speed up the measuring process and simplify the measuring procedure. There is a great wealth of data presented by the Touloukian Series, which generally reports experimental uncertainties of less than 10%.[1] The majority of the measuring procedures used to collect these data are elaborate, requiring major efforts in time and equipment to obtain the desired thermal radiative property over a specified temperature range.

Six major constraints applied to the design of the experimental procedures are (1) a horizontal axis solar furnace is used to heat the samples; (2) the total normal emittance of a surface is to be measured directly at elevated temperatures using the separate blackbody technique described previously; (3) the experimental uncertainty of the measurements are to be on the order of ±15% or less; (4) the experimental setup should be relatively simple and not require a large amount of assembly time; (5) the measuring technique is to be relatively rapid, enabling the determination of seven or eight individual data points at elevated temperatures in eight hours; and (6) the samples will be tested at atmospheric conditions instead of in a vacuum or an inert atmosphere. These constraints, as well as three other assumptions to be discussed, are the basis of the experimental design and procedures used. The experimental setup is shown in Figure 3. Details of the setup are discussed in Section 3.4 of this report.

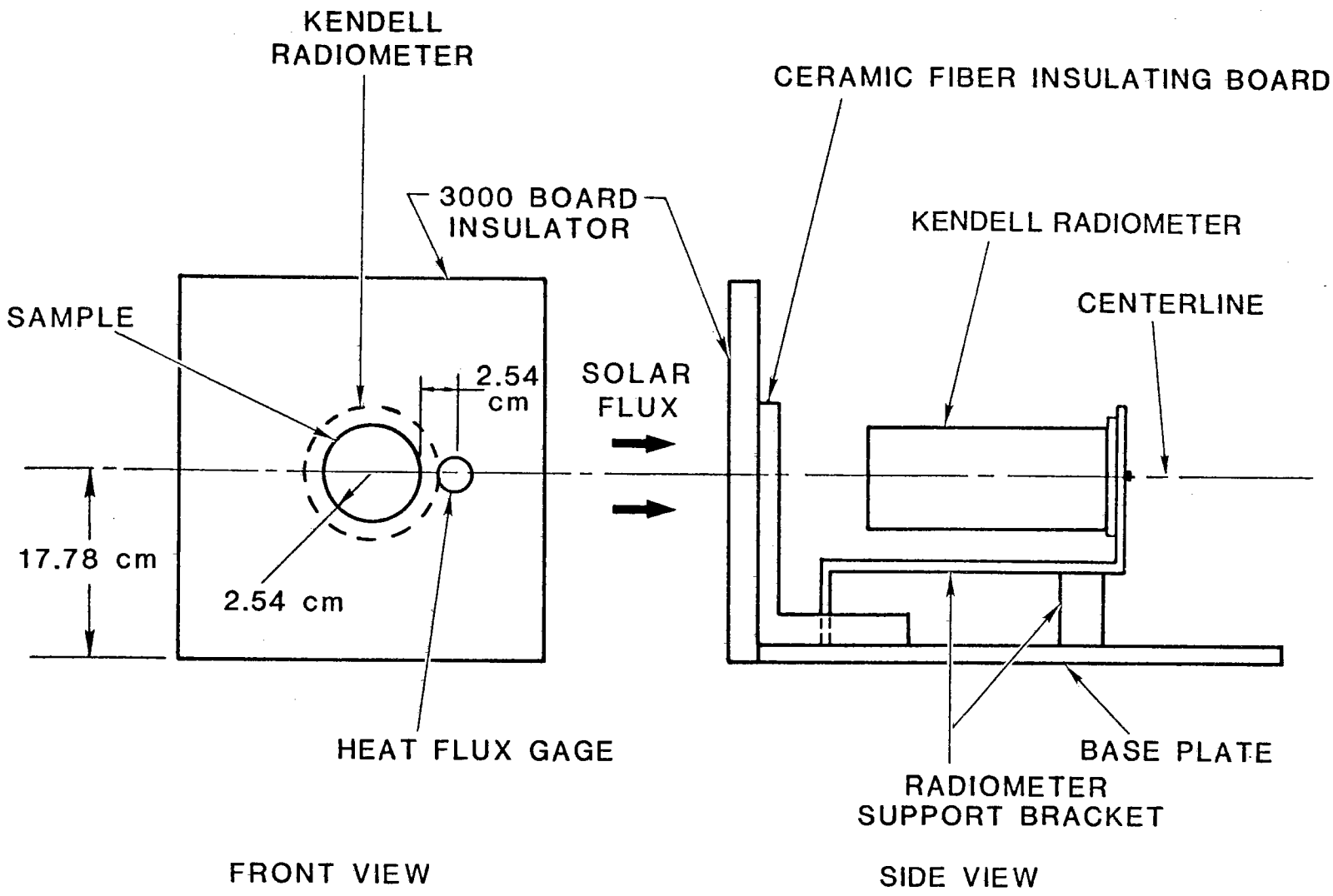

Figure 3. Experimental Setup

3.2 Assumptions

This experiment is based on three controlling assumptions. Each assumption is considered individually, and the experiment is designed such that the errors associated with each are minimal. The three assumptions are as follows:

1. The material is opaque over all wavelengths of the incident radiation,
2. The temperature of the front surface of the material is equal to that of the black surface, and
3. The steady-state temperature is uniform across the surface of the material.

Two metallic materials, aluminum and copper, were chosen to demonstrate the experimental technique. These two materials are opaque over the solar spectrum, and therefore the first assumption will introduce negligible error.

The error associated with the second assumption can be minimized by carefully choosing the material thickness of the sample. If the one-dimensional steady-state heat conduction equation is considered,

$$\frac{d^2T(x)}{dx^2} = 0 \tag{12}$$

along with the boundary conditions,

1. $T(0) = T_h$ (13)

2. $-K \frac{dT(\ell)}{dx} = h(T)\ (T(\ell)-T_{sc}) + \sigma\varepsilon(T)\left(T(\ell)^4-T_{sr}^4\right)$ (14)

then the solution to Eq. 12, 13, and 14 is

$$T(x) = T_h + Ax \tag{15}$$

where A is a real root of

$$A^4 + K_1A^3 + K_2A^2 + K_3A + K_4 = 0 \tag{16}$$

and

$$K_1 = \frac{4T_h}{\ell} \tag{17}$$

$$K_2 = \frac{6T_h^2}{\ell^2} \tag{18}$$

$$K_3 = \frac{4T_h^3}{\ell^3} + \frac{K}{\ell^4\sigma\varepsilon(T)} + \frac{h(T)}{\ell^3\sigma\varepsilon(T)} \tag{19}$$

$$K_4 = \frac{h(T)}{\ell 2\sigma\varepsilon(T)}(T_h - T_{sc}) + \frac{1}{\ell^4}(T_h^4 - T_{sr}^4) \tag{20}$$

(Refer to Appendix C for the derivation of this equation). It should be noted that the first boundary condition assumes that the energy absorbed by the front surface overcomes any losses due to convection and emission, such that the temperature of the front surface is always T_h. A standard HP computer package was used to solve Eq. 16 through 20 for the four roots of the polynomial. The results of this program indicate that two roots are imaginary, one root is a large negative number, and the remaining root is negative and close to zero. By physical reasoning, the small negative root is the only logical choice for a solution since the large negative root would yield infinitely small sample thicknesses. In Table 1 the smallest real roots for four sample thicknesses at the temperature levels of interest are shown. In these calculations, the specific heat of air was assumed to be 100 J/kg °C, the thermal

Table 1

Smallest Real Root of the Polynomial

$$A^4 + K_1A^3 + K_2A^2 + K_3A + K_4 = 0$$

Aluminum Samples

T, °C	ε^*	ℓ = 0.25	ℓ = 0.50	ℓ = 0.75	ℓ = 1.00
300	0.10	-0.0414	-0.0414	-0.0414	-0.0414
400	0.10	-0.0752	-0.0752	-0.0752	-0.0752
500	0.10	-0.1272	-0.1272	-0.1272	-0.1272

Copper Samples

T, °C	ε^*	ℓ = 0.25	ℓ = 0.50	ℓ = 0.75	ℓ = 1.00
300	0.10	-0.0186	-0.0186	-0.0186	-0.0186
400	0.40	-0.1251	-0.1251	-0.1251	-0.1251
500	0.55	-0.2956	-0.2955	-0.2954	-0.2953
700	0.80	-1.0693	-1.0691	-1.0670	-1.0658

"A" has units of K/cm.

"ℓ" is in cm.

*Assumed values for total hemispherical emittance

conductivity of copper and aluminum was assumed to be 1266.3 and 749.6 W/m^2 °C,[12] respectively, T_{sc} and T_{sr} were assumed to be 30°C, and the film coefficients were those defined in the results section of this report. The temperature difference between the front surface of the sample and the back surface can be estimated using Eq. 14. In Table 2, these temperature differences for four sample thicknesses, 0.25, 0.50, 0.75, and 1.0 cm, are shown. The results indicate that for a sample thickness less than 0.75 cm, the temperature drop through the sample is negligible (i.e., approximately within the accuracy of the thermocouples used to measure the temperature of the sample). Therefore, for convenience, a sample thickness of 0.635 cm (0.25 in) was used.

Table 2

Temperature Difference from the Front to the Back Surface

Aluminum Samples

T, °C	ℓ = 0.25	ℓ = 0.50	ℓ = 0.75	ℓ = 1.00
300	0.01	0.02	0.03	0.04
400	0.02	0.04	0.06	0.08
500	0.03	0.06	0.10	0.13

Copper Samples

T, °C	ℓ = 0.25	ℓ = 0.50	ℓ = 0.75	ℓ = 1.00
300	0.00	0.01	0.02	0.02
400	0.03	0.06	0.09	0.13
500	0.07	0.15	0.22	0.30
700	0.27	0.53	0.80	1.07

All temperatures shown are in °C.
"ℓ" is in cm.

The error associated with the third assumption is checked experimentally. A 5.03-cm diameter circular sample of each material was chosen. Each of the samples was instrumented with nine chromel-alumel thermocouples and the temperature across the surface at each temperature level was recorded. If the temperature distribution over the surface is approximately uniform (i.e., within the accuracy of the thermocouple), then the third assumption is justifiable.

3.3 Description of the Solar Furnace

The horizontal axis solar furnace at the Central Receiver Test Facility located at Sandia National Laboratories in Albuquerque, New Mexico, consists of a tracking heliostat, a stationary parabolic concentrator, an attenuator, a remotely

controlled platform for positioning the test items, and a minicomputer for furnace control and data acquisition (Figure 4).[13]

The parabolic concentrator consists of 228 silvered glass mirrors, contoured by the slump-glass method to a spherical shape, which reflect the solar flux received from the heliostat to the focal plane. The concentrator has an opening of 6.7 m^2 with the center 1 m^2 not covered by mirrors. The parabolid has a focal length of 4.6 m and a half-angle of 45°.

The attenuator is a venetian-blind-type structure, which is located between the heliostat and concentrator and is computer-controlled in 90 discrete increments of approximately 0.5 degrees each. The attenuator is used to control the flux density on the test sample and to start and stop an experiment, taking approximately 3 s to close from the full open position.

The test table positions a test sample in the focal plane with a repeatability of better than 0.5 mm in all three dimensions of table movement.

The furnace operation is controlled by a Hewlett-Packard 9845B desktop minicomputer. The computer controls all operations of the furnace, as well as the data scanning and storage. A data acquisition system allows up to 100 channels of thermocouple, voltage, and current data to be scanned, stored, and displayed at the experimenter's command.

3.4 Experimental Apparatus

The experimental apparatus used is shown in Figure 3. The sample disk is held in place by a ceramic fiber insulator board (i.e., 3000 Board*). This 3000 Board is formed from a

*3000 Board is a trade name.

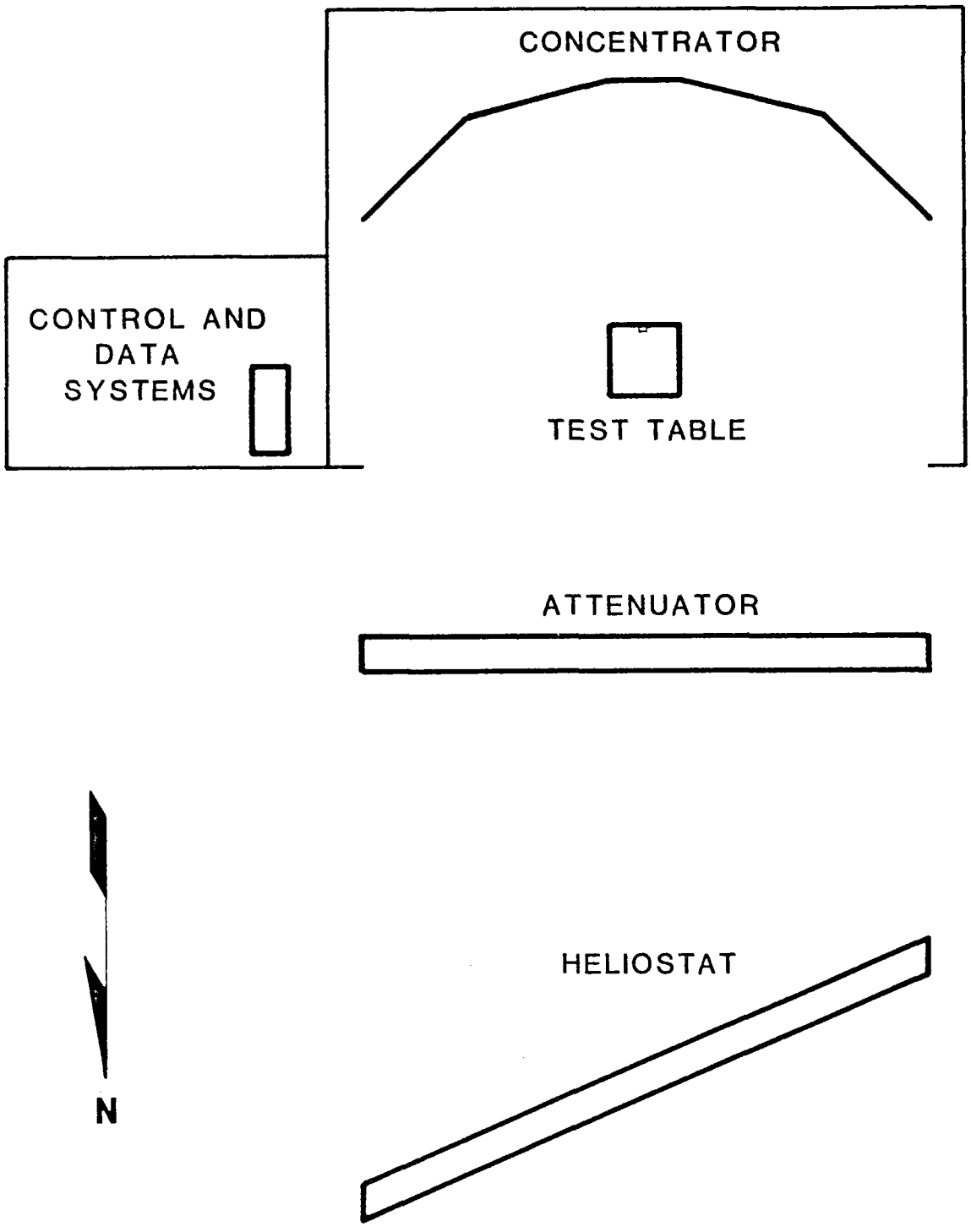

Figure 4. CRTF Solar Furnace

slurry consisting of Kaowool and Saffil and the appropriate quantities of organic and inorganic binders. The board has a melting point of 2144 K (1871°C) and a thermal conductance of approximately 0.0548 W/(m^2 °C) at 973 K (700°C). No metal support, screws, or brackets are used to support the sample, thereby minimizing any associated conduction losses. Thus, the only path for conduction of heat away from the sample is along the two thermocouple wires connected to the sample, assuming that the 3000 Board has a negligible thermal conductivity. The entire length of the thermocouple wires is insulated, essentially eliminating any losses due to convection and emission along the wire. Therefore, losses due to conduction away from the sample by the fin effect are minimal. Also, the edges of the samples are insulated by the 3000 Board such that the heat lost by convection and emission is only from the front and the back surfaces of the sample.

A circular foil heat flux gage is placed 2.5 cm from the edge of the sample (Figure 3). This heat flux gage is used to estimate the thermal power incident upon the front surface of the sample during each test. The gage is calibrated such that a reading taken in the test position can be related directly to the incident thermal power on the sample. The procedure used to calibrate the gage is discussed in Section 4.5.

A Kendell MK-VI Radiometer system is used to measure the total emissive power normal to the sample.[14] The radiometer is a self-calibrating, cavity type with an effective aperture of 0.65 cm. The remaining specifications for the MK-VI radiometer, as well as for the control unit, are listed in Table 3. The front surface of the radiometer is placed 11.9 cm behind the sample surface, resulting in the unit seeing a 2.7-cm-diameter area of the sample. The radiometer is aligned such that its center is along the normal to the center of the sample.

Table 3

Kendell MK-VI System Specifications

Radiometer Specifications

Range	0.02 to 0.4 W/cm^2
Accuracy	±0.5% of reading ±0.1 mW/cm^2
Time constant	6 s (1/e)
Sensitivity	Greater than 10 MV per W/cm^2
View angle	5-degree solid angle

Control Unit Specifications

Accuracy	Absolute measurement uncertainty is less than ±0.5% of the radiometer full-scale range.
Zero drift	0.1% per month of the radiometer full-scale range
Time constant	2 s (1/e)

3.5 Experimental Uncertainty

For every set of measurements taken in this experiment, the mean value and the standard deviation were calculated. Throughout this experimental analysis, the uncertainty of an independent variable is assumed to be the standard deviation of the data set, unless otherwise specified. A Kline-McClintock uncertainty analysis performed on a calculated result r, on the basis of the experimental uncertainty of the measurements taken, is given by

$$w_r = \left\{ \left(\frac{\partial r}{\partial x_1} w_{x_1} \right)^2 + \left(\frac{\partial r}{\partial x_2} w_{x_2} \right)^2 + \ldots + \left(\frac{\partial r}{\partial x_n} w_{x_n} \right)^2 \right\}^{1/2} \quad (21)$$

where w_r is the uncertainty of the calculated result, x_1, x_2, ... , and x_n, are the independent variables, and w_1, w_2, ...,

and w_n, are the uncertainties associated with the measured independent variables.[15] For each calculation made in this experiment, the associated uncertainty is also calculated.

As stated previously, the total normal emittance is the ratio of the emitted energy normal to the real surface to that of a blackbody at the same conditions; that is,

$$\varepsilon_{n(T)} = \frac{e_n(T)}{e_{bn}(T)} \tag{22}$$

and therefore the uncertainty of this calculation is given by

$$w_\varepsilon = \left\{ \left(\frac{1}{e_{bn}} w_{e_n} \right)^2 + \left(\frac{e_n}{-e_{bn}^2} w_{e_{bn}} \right)^2 \right\}^{1/2} \tag{23}$$

4. EXPERIMENTAL PROCEDURES

4.1 Sample Preparation

As discussed in an earlier section, aluminum and copper samples were used to demonstrate the experimental technique. Six Al-6061-T651 aluminum disks, 5.08 cm in diameter and 0.635 cm thick, and six certified oxygen-free, highly conductive, copper disks with the same dimensions were used for testing. The samples were finished to a "visually" shiny surface with 400-grit sandpaper and fine steel wool. Two chromel-alumel thermocouple wires (24-ga) were then peened into holes drilled (#75 drill) on the edge of the sample disk directly across the face from one another to measure the maximum temperature gradient across the sample diameter. Each individual wire of the thermocouple was peened to the sample, making the material a part of the thermocouple junction. This method works quite well and is the most accurate mounting procedure for materials with a high thermal conductivity, and when both junctions are at the same temperature. If the material has a low conductivity, the junction should be made first and then attached to the material sample for an accurate temperature measurement.

Each of the sample disks were cleaned in an ultrasonic bath of water and ordinary dishwashing detergent, rinsed in distilled water, and allowed to dry before sealing in an air-tight container. From this point on, the samples were kept in these containers until the test was performed. Each sample was marked according to the temperature at which it was tested (i.e., 573 K (300°C) = III, 673 K (400°C) = IV, etc.). This numbering scheme is used throughout this report to present the results and identify each sample.

4.2 Temperature Gradient Measurements

One of each of the prepared material samples was used for temperature gradient measurements. The back of each sample was instrumented with nine chromel-alumel thermocouples in the pattern shown in Figure 5. The sample was then placed in the experimental setup shown in Figure 3 and heated, using the solar furnace, to each of the desired temperatures. Temperature measurements were taken for all nine thermocouples at nominal temperatures of 373, 473, 573, 673, and 773 K (100°, 200°, 300°, 400°, and 500°C), respectively. A number of readings were taken at each temperature level to calculate the mean value and standard deviation of the data set.

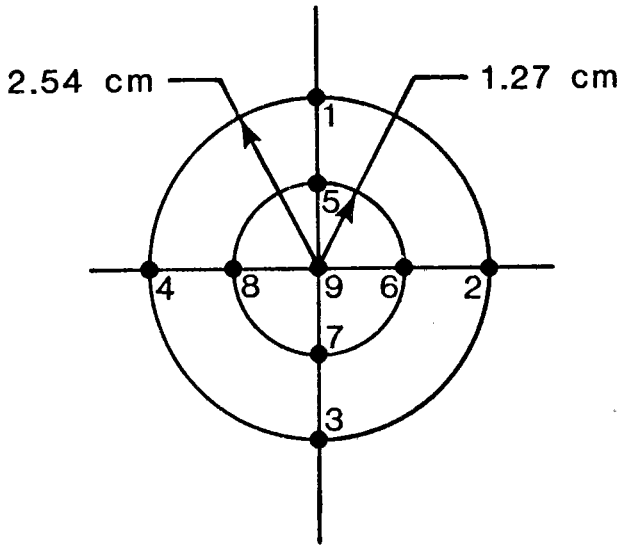

Figure 5. Thermocouple Placement

4.3 Blackbody Calibration

As discussed earlier, a blackbody source made by Barnes Engineering was used as the standard "black" surface. The Kendell radiometer was aligned such that the center axis of the radiometer was along the centerline of the blackbody source. The Kendell was placed 10.2 cm from the front surface of the blackbody aperture. In this configuration, the Kendell

saw a 2.5-cm-diameter disk of the aperture. The blackbody source was then heated to 373, 473, 573, 673, and 773 K (100°, 200°, 300°, 400°, and 500°C) and the corresponding Kendell radiometer readings recorded. Again, a number of readings were taken at each temperature level so the mean value and standard deviation of the data set could be calculated.

The data resulting from this calibration procedure were fit to a second-order polynomial curve of the form

$$KR(T) = A_1 + A_2T + A_3T^2 \qquad (24)$$

where KR(T) is the Kendell radiometer reading of the blackbody, at temperature T. The results of the curve fit indicate that $A_1 = 0.0023115$ W/cm^2, $A_2 = -0.00001389$ W/cm^2 °C, and $A_3 = 2.9564 \times 10^{-8}$ W/cm^2 °C. In Figure 6, the measured data are shown (indicated by the solid circles), as well as the resulting second-order polynomial curve fit through the data. The maximum error between a data point and the curve is 5.4×10^{-5} W/cm^2 and the standard error over all the data is 7.01×10^{-5}.

The Kendell radiometer sees a larger disk of the sample in the experimental mode than when in the calibration mode. However, since the radiometer views the sample only in the experimental mode and the blackbody aperture in the calibration mode, the intensity within the 5-degree solid view angle does not vary. Thus, the Kendell radiometer receives the same intensity in the blackbody calibration mode as it would if the disk viewed by the radiometer were equal to that of the experimental mode.

4.4 Emittance Measurements

Before the emittance of the five remaining samples of each material type was measured, they were taken to the

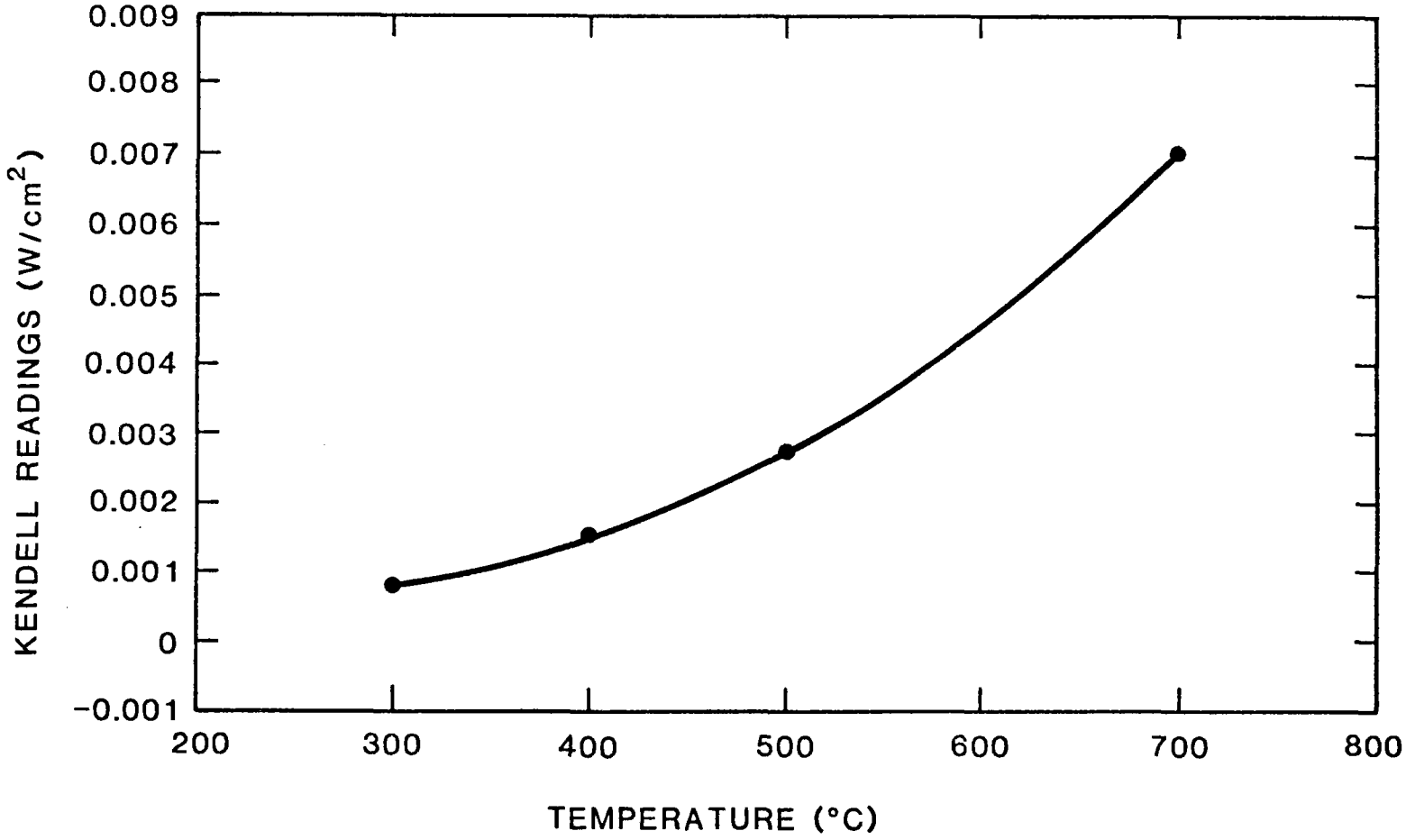

Figure 6. Blackbody Calibration Curve

Thermophysical Properties Division at Sandia National Laboratories, and the total normal emittance was measured at 373 K (100 °C). The experimental procedure outlined below was then used to measure the total normal emittance from 373 to 773 K (100° to 500 °C), at intervals of approximately 100 degrees. Refer to Figure 3 for the location of the elements referred to in the steps below.

1. Mount the circular foil heat flux gage in the experimental apparatus and attach the output lines to the data acquisition system.
2. Attach the Kendell MK-VI Radiometer output line as well as the shielded ambient thermocouple output line to the data acquisition system.
3. Mount a sample in the 3000 Board insulator such that the front surface is flush with the front surface of the 3000 Board.
4. Attach the two thermocouple wires that are connected to the sample to the data acquistion system.
5. Cap the cavity of the Kendell radiometer and take at least six "zero" readings before the testing begins.
6. Remove the cap on the cavity, move the sample into the focal plane, open the attenuator, and heat the sample to the desired steady-state temperature.
7. Take approximately 10 readings, at intervals of 30 s, at this steady-state temperature. A set of data includes the Kendell reading, ambient temperature, the two sample temperature readings, solar radiation, and the reference flux reading.
8. Close the attenuator, and cap the Kendell. Allow approximately 1 min for the Kendell reading to stabilize, then take approximately 10 "zero" readings.
9. Allow the sample to cool to the approximate ambient conditions before removing the sample from the apparatus and sealing.
10. Mount a new sample and repeat the procedure, starting at step 3.

Each sample has one specific temperature level. For instance, aluminum sample III was heated to 573 K (300°C) each time it was tested, while sample IV was heated to 673 K (400°C). In this manner, any oxidation that occurs can be directly associated with the sample temperature level. Each sample was heated to its respective temperature three times from ambient conditions.

A number of data points were taken every time a reading from the Kendell radiometer was made. This was necessary because of a small drift in the output of the Kendell unit due to "noise" in the line and sensing device. The drift was not significant unless very low emittance levels were being measured. It should be noted that the radiometer was designed to record flux levels on the order of 1 sun (1 kW/m^2). Therefore, the drift of approximately 0.01 kW/m^2 becomes insignificant when compared to an incoming flux level. At low emittance (or flux) levels (e.g., less than 0.05 kW/m^2), however, this drift became significant and was accounted for by taking zero readings as well as taking a number of data points and calculating the mean and standard deviation of the data set.

4.5 Flux Field Map

As stated previously, the reference heat flux gage (see Figure 3 for its location) was calibrated such that a flux reading could be converted directly to the total thermal power incident upon the circular sample. In general, the incident flux at or near the focal plane of the concentrator was not constant across the entire field. A two-dimensional flux field map was required to accurately estimate the thermal power incident upon the test sample.

A laser unit was used to align the center of the sample along the centerline of the concentrator at the focal plane. It should be noted here that the samples were aligned at the center of the focal plane in this manner before the emittance

measurements began. With the sample at this central position, the attenuator was opened and the reference flux reading was recorded. The center point of the sample now constitutes the center of the flux field. The heat flux gage was moved to this central position, and using a scanning program for the HP9845B, the 6.6-cm, two-dimensional flux field was mapped by recording the heat flux gage readings in increments of 0.5 cm across the field.

The 196 data points taken in this flux map were then used to estimate the total thermal power on the sample surface. A numerical integration routine was used to estimate the thermal power within a 2.54-cm-radius circle. This program assumes that the flux was constant over an incremental square ±0.25 centimeters, in both dimensions, about the location of the data point. This integration routine is accurate to within ±5% of the actual thermal power incident upon the sample for this data spacing. Therefore, the resulting thermal power was related directly to the reference flux reading. A calibration factor (C.F.) can then be defined as the ratio of the incident thermal power to the normalized reference flux reading; that is,

$$\text{C.F.} = \frac{\text{incident total thermal power}}{\text{normalized reference flux}} . \qquad (25)$$

If a direct linear relationship between the reference flux reading and the incident thermal power at each attenuator setting is assumed, the above calibration factor can be used to estimate the thermal power on the sample during each test.

5. RESULTS AND DISCUSSION

The presentation of the experimental results is divided into three separate sections, as follows: (1) temperature difference measurements, (2) incident flux field mapping, and (3) total normal emittance measurements.

5.1 Temperature Difference Measurements

As described in a previous section, nine thermocouples were used to measure the temperature distribution across the sample surface. The temperature difference between the center of the sample and the measured temperature at the outer two radii of the sample (refer to Figure 5 for thermocouple placement) is shown in Table 4. Since the accuracy of the chromel-alumel thermocouples is approximately ±1.0 degree, the majority of the temperature measurements are within the thermocouple accuracy. These results generally indicate a negligible temperature distribution across the sample surface. As a result, the assumption of a uniform constant temperature across the sample surface is validated within ±1 degree.

5.2 Flux Field Map

The normalized flux (normalized to 1 kW/m^2) field map of the incoming solar flux measured experimentally is shown in Figure 7. This is a 6.6-cm-square field and was mapped at an attenuator position that produced approximately one-sixth of the maximum thermal power of the solar furnace. This flux level was chosen because it represents the approximate mean setting during the course of testing. Figure 8 is an isoflux map of this measured data. Each line represents the indicated percentage of the peak flux measured in the field. The sample

Table 4

Measured Temperature Difference from Central Thermocouple (#9) on the Front Surface

Copper

#1*	#3	#9	#4	#2
+0.1	+0.2	140	-0.7	+0.4
+0.6	+0.1	218	-0.4	+0.3
+1.6	+0.5	300	+0.7	+0.5
+4.3	+0.8	398	+1.5	+0.8
+0.6	+1.2	495	0.0	+1.1

Aluminum

#1*	#3	#9	#4	#2
-1.3	0.0	145	-0.3	-0.8
-1.1	-0.0	232	-0.3	-0.8
-0.9	-0.1	309	-0.4	-0.8
-1.5	+0.4	407	-0.5	-0.9
-1.1	+0.8	495	-0.8	+0.2

*Refer to Figure 5 for the thermocouple numbers shown

Center column is temperature in °C; other columns are temperature difference in °C.

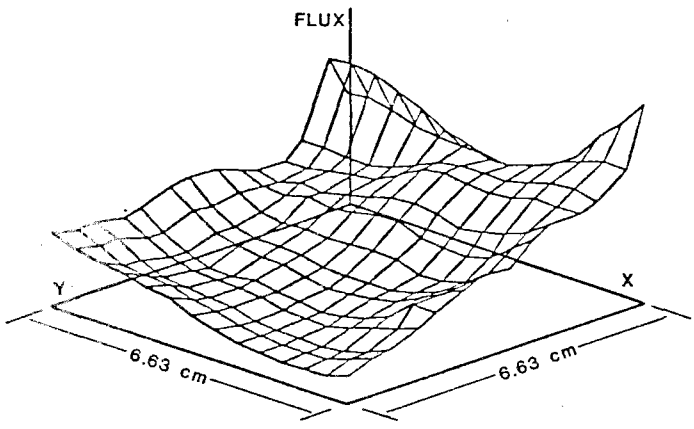

Figure 7. Three-Dimensional Plot of the Incoming Flux Field

diameter is also shown in Figure 8, giving one an idea of the incident flux field upon the front surface of the sample. These flux measurements were used to calculate the normalized power incident upon the sample by using the numerical integration routine.

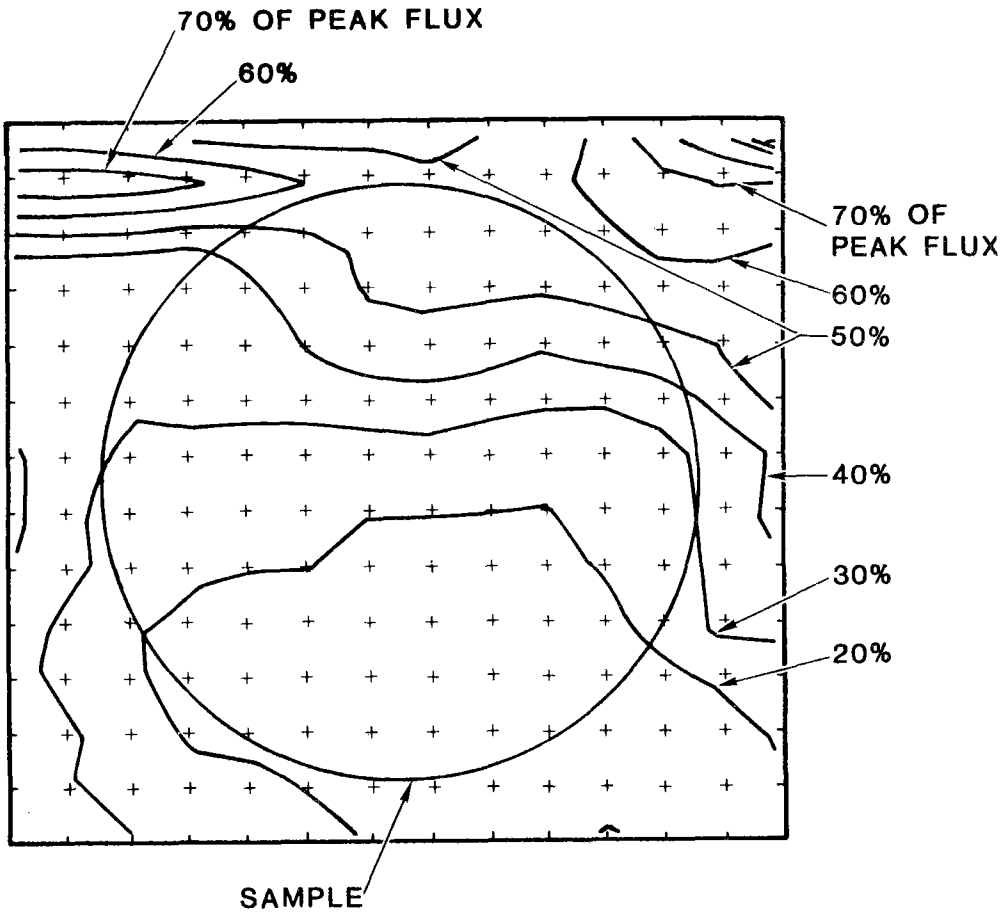

Figure 8. Isoflux Plot with Sample Superimposed

The results of this numerical integration indicate that approximately 4.21 W thermal were incident upon the 5.08-cm-diameter circular sample. Noting that the average

normalized reference flux measurement was 5.13 W/cm^2, we can calculate the calibration factor using Eq. 25 as 0.820 $W_{thermal}/(W/cm^2)$. This calibration factor was normalized to 1 sun (1 kW/m^2) and thus the reference flux measurements during testing must also be normalized to 1 sun before the calibration factor is used. The normalized thermal power incident upon the sample is calculated by multiplying the calibration factor by the normalized reference flux measurement. Further, the actual thermal power incident upon the sample is found by multiplying this value by the insolation at the testing site; that is,

$$Q_t = (\text{C.F.})(\text{Norm. Ref. flux})(\text{Insolation}) \ . \qquad (26)$$

Although the flux distribution of the incoming solar radiation is not uniform across the sample, the results presented in Section 5.1 indicate that the effect on the temperature nonuniformity is negligible.

5.3 Total Normal Emittance Measurements

The measured total normal emittance of aluminum at 573, 673, and 773 K (300°, 400°, and 500°C) is shown in Figure 9. The table shown in this figure presents the plotted data ε_n, as well as the corresponding experimental uncertainty, w_ε, as calculated by Eq. 23. The total normal emittance of aluminum at 373 and 473 k (100° and 200°C) was also measured using this experimental technique and was found to be 0.33 and 0.12, respectively. These values do not follow general trends of presently published data and are not in agreement with measurements taken at 373 K (100°C) by the Thermophysical Properties Division with a Gier-Dunkel infrared reflectometer (Appendix A). The directional emissive power of aluminum was very low at these temperatures and, as previously discussed, the Kendell MK-VI Radiometer System has a drift due to noise in the line and sensing device. The drift is on the order of the total normal emissive power of aluminum at 373 K (100°C)

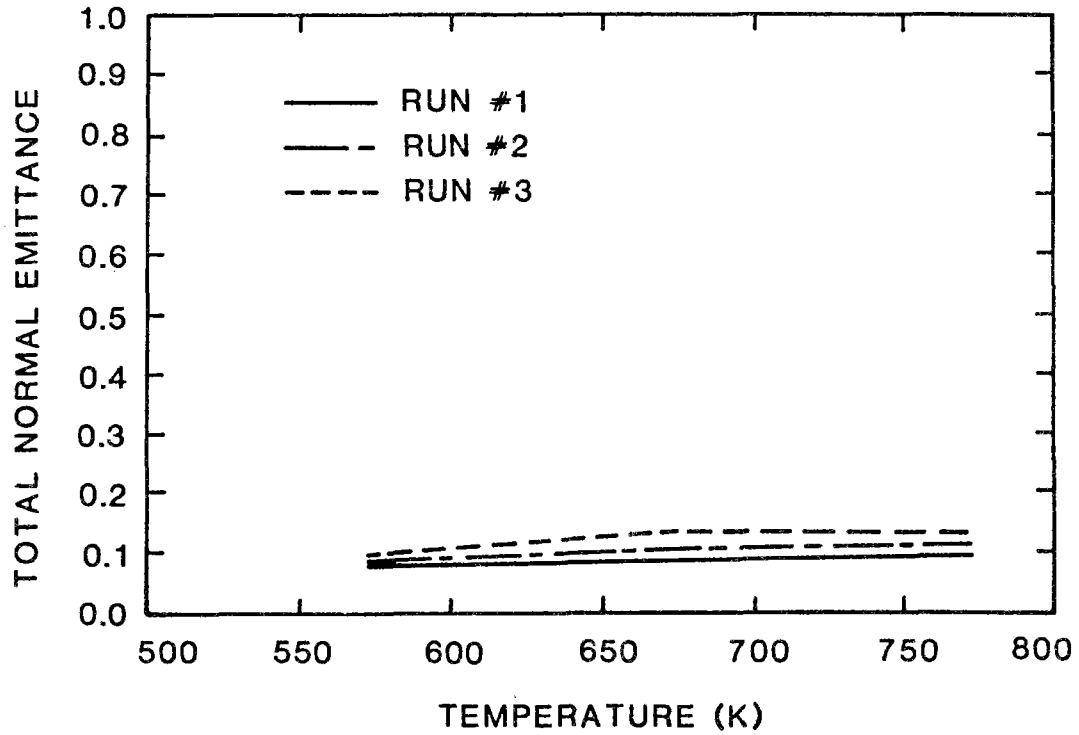

SAMPLE	T_h (K)	ϵ_n	w_{ϵ_n}
AL-III---1	585	0.08	0.01
AL-IV---1	675	0.09	0.03
AL-V---1	779	0.10	0.01
AL-III--2	575	0.09	0.02
AL-IV--2	674	0.11	0.01
AL-V---2	776	0.12	0.02
AL-III--3	577	0.10	0.02
AL-IV--3	669	0.14	0.02
AL-V---3	775	0.14	0.01

Figure 9. Total Normal Emittance of Aluminum

and therefore the measure emittance values at 373 and 473 K (100° and 200°C) were not dependable readings and are not presented as part of the final results. Recommendations for instrumentation to reduce or eliminate this problem will be discussed in the last section of this report.

The measured total normal emittance of copper at 573, 673, and 773 K (300°, 400, and 500°C) is shown in Figure 10. This figure includes a table of the experimental values as well as the experimental uncertainty. As with the aluminum samples, the measured total normal emissive power of copper at 373 and 473 K (100° and 200°C) was on the order of the noise drift of the instrument. The total normal emittance measured by the Thermophysical Properties Division (Appendix A) did not compare favorably to these measurements for the same reasons previously discussed for aluminum. As a result, the data are not presented as a part of the final results.

Reference 1 contains data for the normal emittance of aluminum and copper that has been compiled and tabulated from a number of sources. The curves for aluminum, taken from Reference 1, are shown in Figure 11.

The emittance data measured in these tests are all on the order of 0.1. Comparing these data points to the compiled data in Figure 12 indicates that the experimental data fall into the middle-to-upper region of the curves but well within the scatter of the published data.

The data curves for copper compiled by Touloukian are shown in Figure 12.[1] These curves have been analyzed and reduced into general trends (Figure 13), and these trends will be used to compare the trends of the data developed in these experiments. For convenience, the experimental results are plotted in Figure 13 for direct comparison. Note that the samples were all prepared in the same manner before testing,

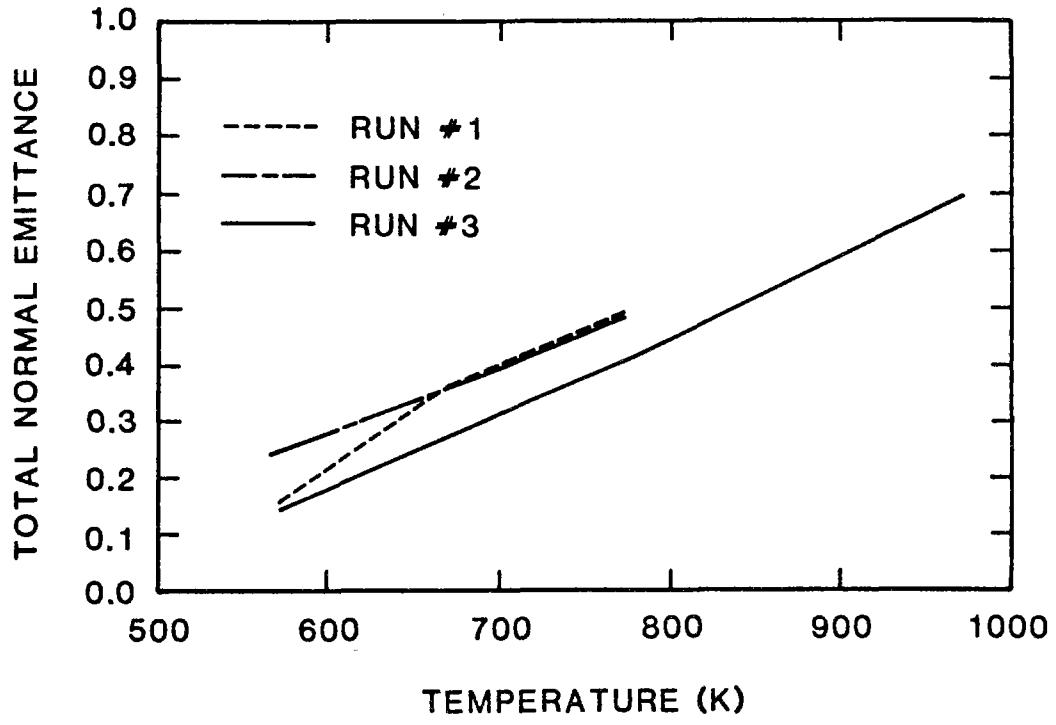

SAMPLE	T_h (K)	ϵ_n	w_{ϵ_n}
CU-III--1	571	0.14	0.01
CU-IV--1	674	0.28	0.03
CU-V---1	773	0.41	0.03
CU-I----1	968	0.70	0.07
CU-III--2	575	0.25	0.02
CU-IV--2	673	0.36	0.01
CU-V---2	770	0.50	0.03
CU-III--3	576	0.16	0.02
CU-IV--3	677	0.37	0.01
CU-V---3	773	0.49	0.03

Figure 10. Total Normal Emittance of Copper

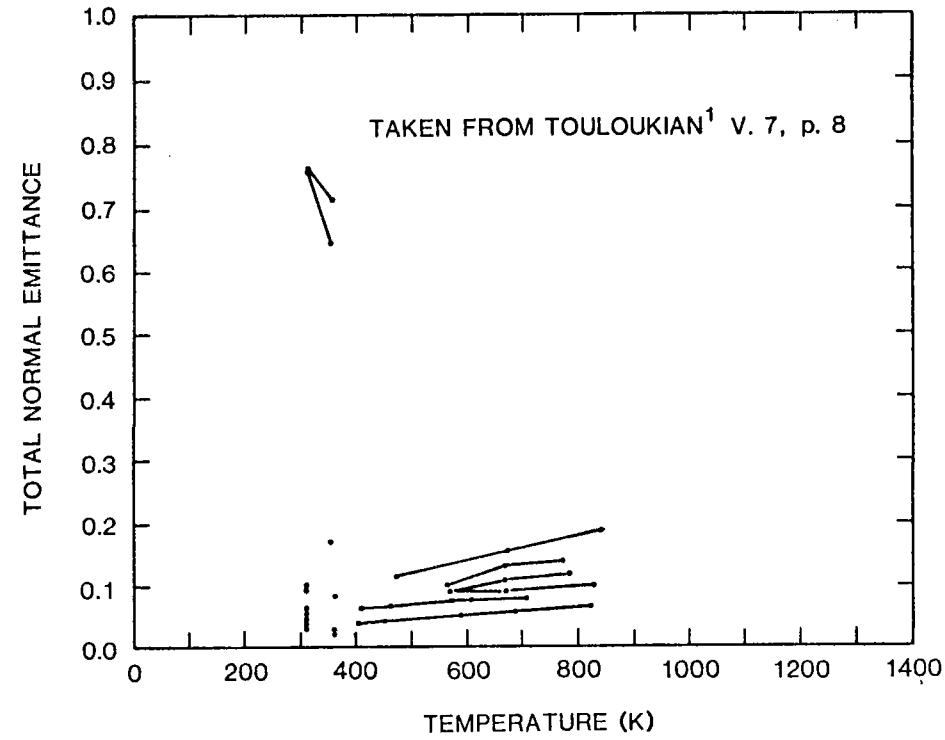

Figure 11. Touloukian Total Normal Emittance of Aluminum

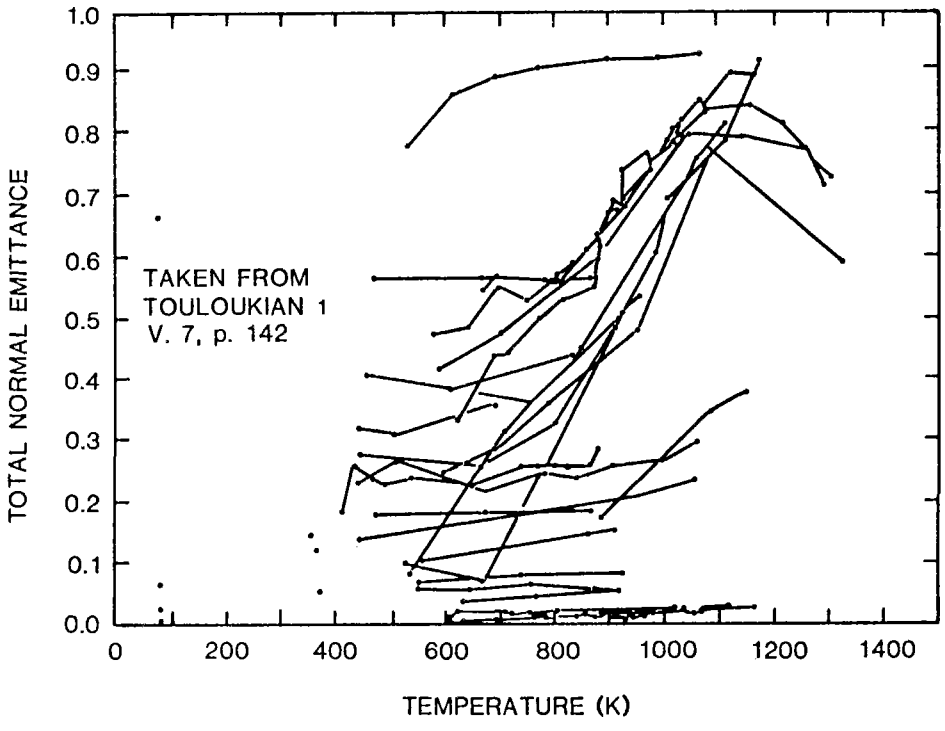

Figure 12. Touloukian Total Normal Emittance of Copper

and each sample has its own temperature level, thus reaching an oxidation level directly related to the temperature of that sample. This oxidation film directly affects the radiative properties of the surface as the film builds up to greater thicknesses at higher temperatures, thereby increasing the emittance of the surface. These trends are not particularly true for all materials, only for the two metal samples evaluated in this report. As shown in Figure 13, the experimental data developed herein follow these general trends and seem to fall into the general neighborhood of the analyzed normal total emittance curves for oxidized and lightly oxidized copper samples.

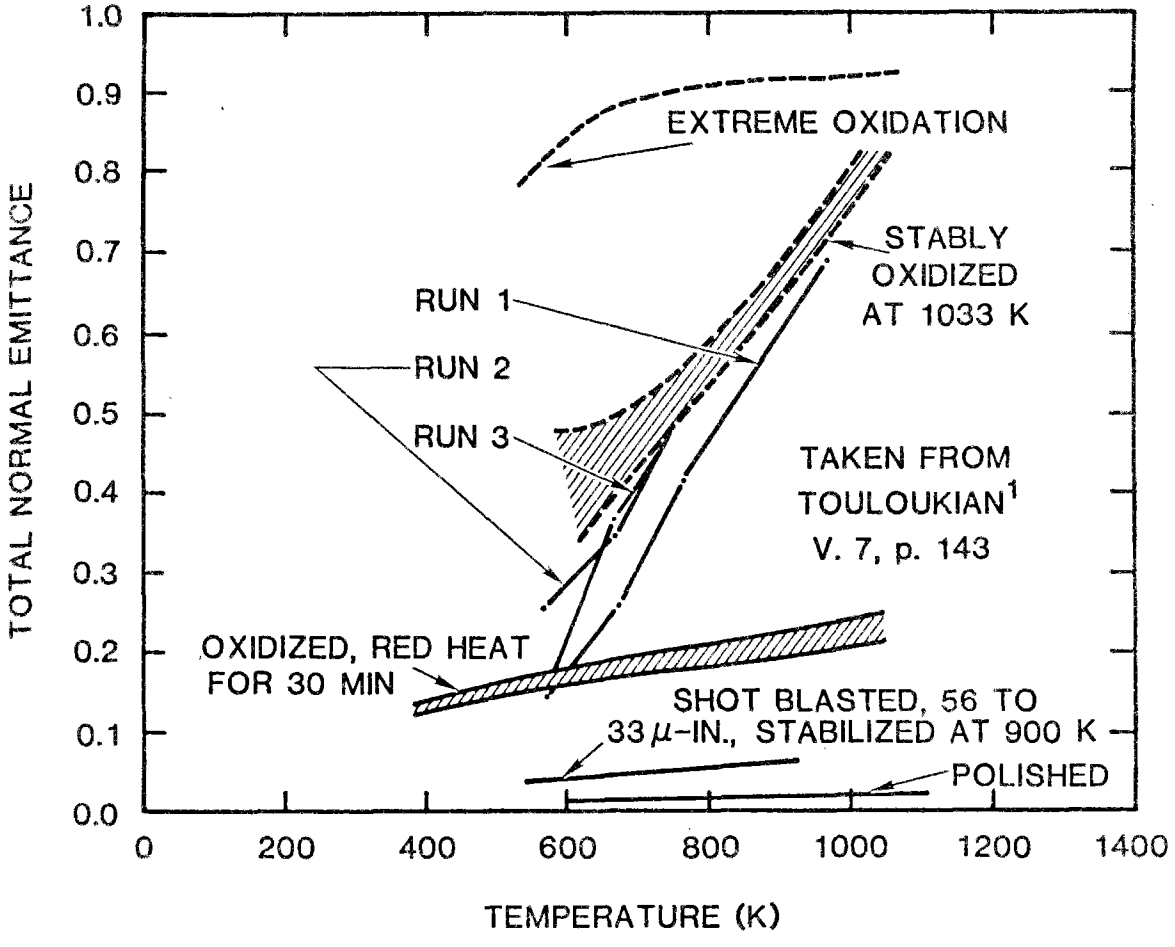

Figure 13. Analyzed Total Normal Emittance of Copper

The experimental technique was also used to measure the total normal emittance of two surface coatings. Aluminum and copper samples were coated with Pyromark Series 2500 black and white paints (manufactured by the Tempil Corp.), and the total normal emittance was measured at 573, 673, and 773 K (300°, 400°, and 500°C), respectively. The Pyromark Series 2500 paint is formulated from 100% silicone resin and is advertised as being able to resist blistering, peeling, and chipping at temperatures up to 1644 K (1371°C).[16] The experimentally measured total normal emittance of these paints over the specified temperature range is shown in Figure 14. These results indicate that the total normal emissive power of the black paint is very close to, and in one case greater than, the total normal emissive power of a blackbody in the same geometric configuration and temperature. The results for the case when the emittance is greater than unity cannot be valid since the total emittance of any surface can never be greater than that of an ideal blackbody. When the radiometer was calibrated with the blackbody source, it viewed a 2.5-cm-diameter disk. When the radiometer was in the experimental mode, it viewed a 2.7-cm-diameter disk. Furthermore, the blackbody source has an effective aperture of 2.54 cm, which is just slightly larger than the 2.5-cm viewing disk of the Kendell radiometer when calibrated. These two factors could affect the output reading of the radiometer and cause the blackbody reading to be somewhat less than that of an ideal blackbody because of nonhomogeneity at the blackbody source aperture. These are offered as suggestions only and not as sources of errors that have been rigorously analyzed. As previously stated, suggestions for instrumentation to eliminate these problems, as well as the others, will be presented in the last section of this text.

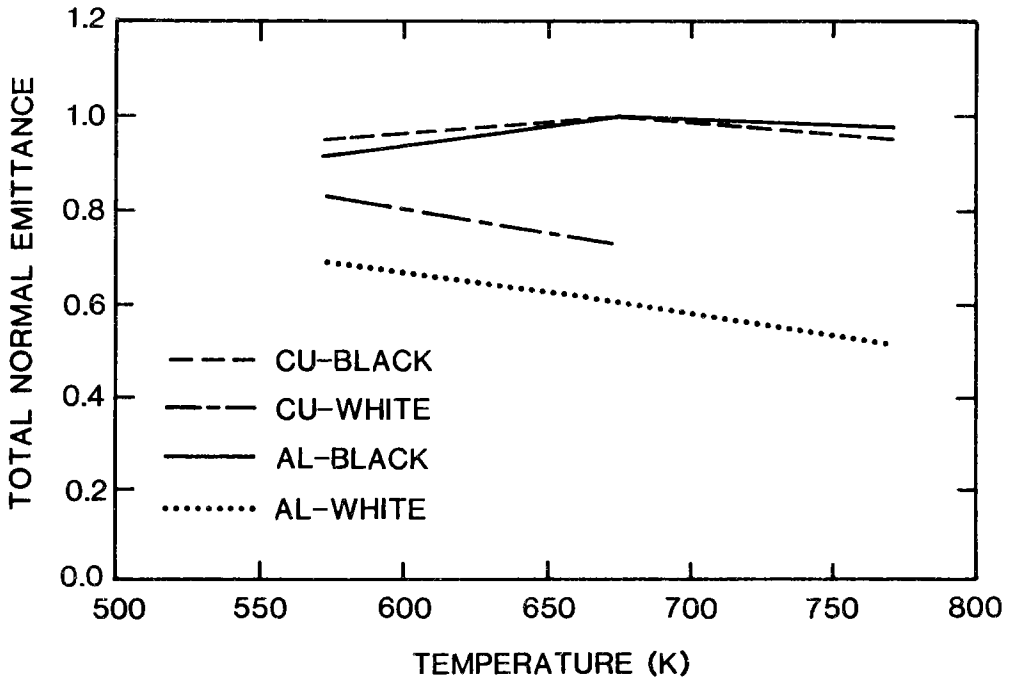

SAMPLE	T_h (K)	ϵ_n	w_{ϵ_n}
CU-BLACK	572	0.95	0.1
CU-BLACK	677	1.1*	0.1
CU-BLACK	775	0.95	0.1
CU WHITE	582	0.83	0.1
+ CU-WHITE	674	0.73	0.1
AL-BLACK	578	0.92	0.1
1 AL-BLACK	673	1.0	0.1
AL-BLACK	768	0.98	0.1
AL-WHITE	573	0.69	0.1
AL-WHITE	681	0.61	0.1
AL-WHITE	778	0.51	0.1

+ PAINT BURNED OFF OF SURFACE AT 673 K
1 COOLING DATA ONLY
* ASSUMED TO BE 1.0 ON PLOT

Figure 14. Total Normal Emittance of Pyromark Coatings

6. CONCLUSIONS

The objective of this experiment was to develop a method to measure the total normal emittance of opaque materials in a solar environment. The results of the experimental measurements at temperatures of 573 K (300°C) and above follow the general trends of the published data for both aluminum and copper with experimental uncertainties between 10% and 15%. At these temperatures, the instrumentation presently available at the Central Receiver Test Facility can be used to estimate the emittance of highly conductive opaque materials. In the case of the aluminum samples, the total normal emittance values (at temperatures exceeding 573 K [300°C]) were all well within the range of emittance values reported in the literature. These results indicate that the experimental procedure has validity, even for low emitters. If a more sensitive radiometer were available, lower emittances could be measured with a greater overall accuracy. The results for the copper samples compare rather well with the analyzed emittance values (Figure 13) compiled by Touloukian.[1] As surface oxidation increased, the emittance of the copper surface also increased. This result is clearly evident in Figure 13, since the black oxidation layer becomes more extreme at higher temperatures. The emittances of the painted surfaces were reasonable when compared to the manufacturer's data. The black surface was a very high emitter, approaching the blackbody condition. The white surface was a relatively high emitter, considering the properties of the coating. Thus, the experimental method works quite well for relatively low, as well as high, emitting surfaces with an uncertainty of 15% or less. For surfaces at temperatures below 573 K (300°C), the experimental data did not follow the published data and were not presented as part

of the final results. At these temperatures, the total normal emitted energy is very low and could not be accurately measured with the Kendell MK-VI Radiometer. Instrumentation much more sensitive to low-level infrared radiation is needed to measure the directional emitted energy below 573 K (300 °C).

7. RECOMMENDATIONS

The major limitation of the experimental technique presented was the radiometer. As mentioned, the cavity-type radiometer system was designed for incoming flux levels on the order of 1 sun. The flux levels measured in this experiment were approximately one-tenth of this level. At sample temperatures below 573 K (300 °C), the flux measured by the radiometer was too low to obtain reliable, accurate results. At sample temperatures of 573 K (300 °C) and above, the results are reliable, compared with other published data. A radiometer sensitive to low-level infrared radiation would extend the capability of this technique to lower temperatures and improve the experimental accuracy at elevated temperatures.

This experimental technique can be modified slightly to measure the reflectance of an opaque material directly. These measurements were not taken since two radiometers were not available. If available, they would have been positioned on opposing sides of the sample such that they viewed the same sample area. The radiometer in back of the sample would measure the emitted radiation of the sample, while the one in front of the sample would measure the reflected plus emitted radiation (while the sample is being irradiated). Thus, the reflected radiation could be separated from the emitted radiation since the front and back surfaces are at essentially the same temperature and thus emit energy equally (care must be taken to prepare each side in the same manner). The reflectance is then calculated as the ratio of the reflected radiation to the incident radiation measured in the same geometric conditions (i.e., directional or hemispherical, depending upon the desired property).

APPENDIX A

Total Normal Emittance Data at 373 K (100°C) (Measured with a Gier-Dunkel Infrared Reflectometer)

This appendix presents the total normal emittance data at 373 K (100°C), which was measured by the Thermophysical Properties Division of Sandia National Laboratories in Albuquerque, New Mexico. These measurements were recorded using a Gier-Dunkel Infrared Reflectometer. The measurement head of this instrument incorporates a rotating cavity that is divided into two semicylindrical chambers and painted black. As the cylinder rotates, a sample placed over the measurement window is alternately irradiated by blackbody radiation corresponding to each cavity temperature. Thus, the thermopile detector receives both infrared radiation emitted by the sample.[17] Below are the measured emittance values at 100°C before testing began, after the first run and when the testing was completed, for the aluminum and copper samples. Also shown are the emittance values before and after testing for the Pyromark coatings.

Measured Emittance Values at 100°C

Data before Testing		Data after First Run		Data after Third Run	
Sample	Emittance	Sample	Emittance	Sample	Emittance
Cu-I	0.026	Cu-I	0.023	Cu-III	0.178
Cu-II	0.029	Cu-II	0.030	Cu-IV	0.310
Cu-III	0.026	Cu-III	0.133	Cu-V	0.288
Cu-IV	0.027	Cu-IV	0.205	Al-III	0.060
Cu-V	0.030	Cu-V	0.280	Al-IV	0.052
Al-I	0.040	Al-I	0.041	Al-V	0.073
Al-II	0.040	Al-II	0.040		
Al-III	0.060	Al-III	0.057		
Al-IV	0.052	Al-IV	0.048		
Al-V	0.042	Al-V	0.052		

Pyromark Series 2500 Data

Data before Testing		Data after Testing	
Sample	Emittance	Sample	Emittance
Cu-Black	0.792	Cu-Black	0.780
Cu-White	0.784	Cu-White	-----
Al-Black	0.821	Al-Black	0.813
Al-White	0.733	Al-White	0.710

APPENDIX B

Conduction and Convection Losses

At steady-state conditions, the energy balance can be expressed as

$$\text{Absorbed energy} = \text{Radiated energy} + \text{Convected Energy} + \text{Conducted Energy} . \quad \text{(B1)}$$

Since the Rayleigh Number is less than 10^9 (on the order of 10^8), the convected energy away from the sample is assumed to be due to laminar free convection past a verticle flat surface over the desired temperature range, as shown in Figure B1.[18]

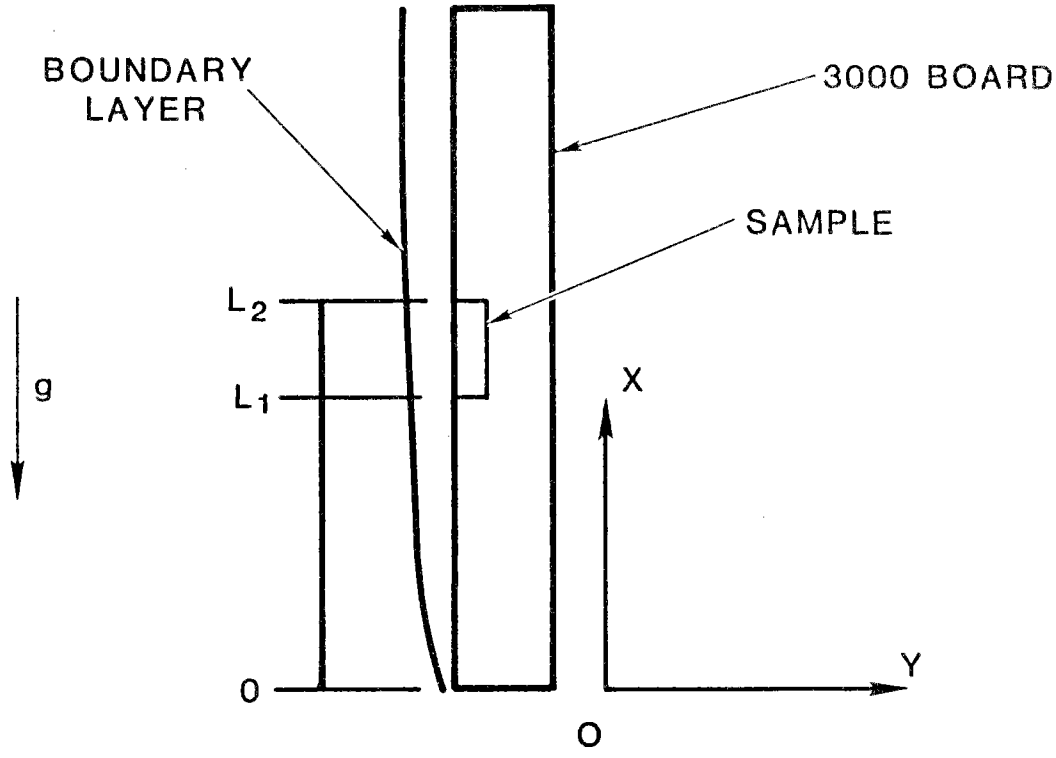

Figure B1. Vertical Plate Coordinate System

From work by Schmidt and Beckmann, which is outlined by Chapman,[12] the local heat transfer coefficient, $h_x(T)$, is given by

$$h_x(T) = \frac{k}{\sqrt{2}} \left[\frac{g\beta\Delta T}{\nu^2 x}\right]^{1/4} f(N_{pr}) \qquad (B2)$$

As shown in Figure B1, the sample is placed a distance L_1 from the bottom of the 3000 board. If we assume that the 3000 board and sample are at a uniform temperature T, then the local heat transfer coefficient can be integrated from L_1 to L_2, to give

$$h(T) = \frac{k}{\sqrt{2}} \left[\frac{g\beta\Delta T}{\nu^2}\right]^{1/4} f(N_{pr}) \int_{L_1}^{L_2} x^{-1/4} dx \qquad (B3)$$

or

$$h(T) = \frac{4k}{3\sqrt{2}} \left[\frac{g\beta\Delta T}{\nu^2}\right]^{1/4} (L_2^{0.75} - L_1^{0.75}) f(N_{pr}) \qquad (B4)$$

In Eq. B1 through B3, β is the coefficient of volume expansion of air and equal to T^{-1} for an ideal gas,[19] ν is the kinematic viscosity of air at temperature T, g is the local gravitational constant, $\bar{k}$ is the thermal conductivity of air at temperature T, T is the temperature of the vertical plate, T_∞ is the temperature of fluid far removed from the plate, $\bar{T}$ is the average temperature, $1/2(T + T_\infty)$, $f(N_{pr})$ is the function

$$f(N_{pr}) = \frac{0.676\ N_{pr}^{1/2}}{(0.861 + N_{pr})^{1/4}} \qquad (B5)$$

and N_{pr} is the Prandtl number equal to $(\mu^* C_p/k)$.

The film coefficient was calculated using Eq. B4 and B5, and the results of these calculations are shown below in Table B1.

Table B1

Film Coefficients

T (°C)	h(T), W/(cm^2 °C)
300	0.00299
400	0.00313
500	0.00323
700	0.00335

The conduction losses from the sample to the 3000 board insulator are now considered. If the 3000 Board is assumed to be homogeneous and if the predominant mode of energy transportation is by conduction, then the radial heat flow from the sample to the 3000 is given by[12]

$$q_r = \frac{2\ ct^2(T_i - T_o)}{\ln(r_o/r_i)} \qquad (B6)$$

where T_i is the sample temperature, T_o is the temperature at the outer edge of the 3000 Board, r_i is the sample radius, r_o is the radius of the outer edge of the 3000 Board, c is the thermal conductance of the 3000 Board, and t is the thickness of the sample. If as a limiting case, we let

$$T_i = 700\,°C$$
$$T_o = 100\,°C$$
$$r_i = 2.54\ cm$$
$$r_o = 15.24\ cm$$
$$c = 1.009 \times 10^{-3}\ W/cm\ °C\ ,$$

then the heat conducted radially away from the sample is

$$q_r = 0.87 \text{ W} ,$$

which is negligible in comparison to the incoming flux as well as the energy convected and radiated away from the surface.

APPENDIX C

Solution to Temperature Distribution

For a sample that is uniform in temperature, with no internal heat generation and one-dimensional conduction, the general heat conduction equation reduces to

$$\frac{d^2T(x)}{dx^2} = 0 \ , \tag{C1}$$

which has a solution of

$$T(x) = A\ x + B \ . \tag{C2}$$

If the incoming solar flux, q, is such that the temperature of the front surface is constant at steady state and the heat loss from the back surface is due to laminar free convection and thermal radiation, then the boundary conditions can be expressed as

$$1. \quad T(0) = T_h \tag{C3}$$

$$2. \quad -K \frac{dT(\ell)}{dx} = h(T)(T(\ell) - T_{sc}) + \sigma\varepsilon(T)(T(\ell)^4 - T_{sr}^4) \tag{C4}$$

If we now use these boundary conditions to evaluate the constants A and B in Eq. B2, then

$$1. \quad T(0) = A(0) + B = T_h \qquad B = T_h \tag{C5}$$

and therefore

$$T(x) = Ax + T_h \tag{C6}$$

The second boundary condition, Eq. C4, yields

$$2.\ -KA = h(T)(A\ell + T_h - T_{sc}) + \sigma\varepsilon(T)((A\ell + T_h)^4 - T_{sr}^4) \tag{C7}$$

or

$$-(K + h\ell)A = h(T)(T_h - T_{sc}) + \sigma\varepsilon(T)((A\ell + T_h)^4 - T_{sr}^4)\ . \tag{C8}$$

Now as we expand the term

$$(A\ell + T_h)^4 \tag{C9}$$

we have

$$(A\ell + T_h)^4 = (A\ell)^4 + 4T_h(A\ell)^3 + 6T_h^2(A\ell)^2 + 4T_h^3(A\ell) + T_h^4 \tag{C10}$$

Substitution of Eq. C10 and C8 into Eq. C7 and rearranging gives

$$A^4 + \left(\frac{4T_h}{\ell}\right)A^3 + \left(\frac{6T_h^2}{\ell^2}\right)A^2 + \left[\frac{4T_h^3}{\ell^3} + \frac{K}{\ell^4\sigma\varepsilon} + \frac{h}{\ell^3\sigma\varepsilon}\right]A$$

$$+ \frac{h}{\ell^4\sigma\varepsilon}(T_h - T_{sc}) + \frac{1}{\ell^4}(T_h^4 - T_{sr}^4) = 0\ , \tag{C11}$$

which is in a form such that it can be solved numerically for the four roots.

REFERENCES

1. Y. S. Touloukian and D. P. Dewitt, ed, Thermal Radiative Properties--Metallic Elements and Alloys, Thermophysical Properties of Matter, TPRC Data Series Volume 7, IFI Plenum, New York, 1970, pp. 29a-42a.

2. D. G. Moore, "Investigation of Shallow Reference Cavities for High Temperature Emittance Measurements," Measurements of Thermal Radiative Properties of Solids, J. C. Richmond, ed, NASA-SP-31, 1963, pp. 515-525.

3. J. C. Richmond, W. N. Harrison, and F. J. Shorten, "An Approach to Thermal Emittance Standards," Measurements of Thermal Radiative Properties of Solids, J. C. Richmond, ed, NASA-SP-31, 1963, pp. 403-423.

4. A. Gravina, R. Bastian, and J. Dyer, "Instrumentation for Emittance Measurements in the 400° to 1800°F Temperature Range," Measurement of Thermal Radiative Properties of Solids, J. C. Richmond, ed, NASA-SP-31, 1963, pp. 329-336.

5. R. B. Pettit and R. R. Sowell, "Solar Absorptance and Emittance Properties of Several Solar Selective Coatings," J. Vac. Sci. Technol., Vol. 13, 1976, pp. 596-602.

6. R. B. Pettit, Total Hemispherical Emittance Measurement Apparatus for Solar Selective Surfaces, SAND75-0079 (Albuquerque: Sandia Laboratories, 1975).

7. J. R. Grammer and E. R. Streed, "Measurement of Normal and Directional High Temperature Total and Spectral Emittance," Measurement of Thermal Radiative Properties of Solids, NASA-SP-31, 1963, pp. 489-498.

8. R. J. Evans, W. A. Clayton, and M. Fries, "A Very Rapid 3000°F Technique for Measuring Emittance of Opaque Solid Materials," Measurement of Thermal Radiative Properties of Solids, NASA-SP-31, 1963, pp. 483-488.

9. J. N. Sweet and R. B. Pettit, Optical Modeling of Black Chrome Solar Selective Coatings, SAND82-0964, (Albuquerque: Sandia National Laboratories, 1982).

10. J. R. Howell and R. Siegel, Thermal Radiation Heat Transfer, (2nd ed; New York: McGraw-Hill Book Co., 1972), pp. 17-18.

11. W. G. Driscoll and W. Vaughan, Handbook of Optics, (New York: McGraw-Hill Book Co., 1978), pp. 3-12.

12. A. J. Chapman, Heat Transfer (3rd ed; New York: Macmillan Publishing Co., Inc., 1974).

13. J. T. Holmes and R. M. Edgar, "The Horizontal Axis Solar Furnace at the Central Receiver Test Facility," for publication in High Temperature Technology, (Albuquerque: Sandia National Laboratories, 1982).

14. J. Kendell, Instruction Manual for the Kendell Radiometer System, Pasadena, CA: Technical Measurements, Inc., Jet Propulsion Labs, 1978).

15. J. P. Holman, Experimental Methods for Engineers, (3rd ed; New York, McGraw-Hill Book Company, 1978).

16. "High Temperature Coatings for Space," Modern Paint and Coatings, Tempil Division, Big Three Industries, Inc., South Plainfield, New Jersey, 1978.

17. R. B. Pettit, "Evaluation of Portable Optical Property Measurement Equipment for Solar Selective Surfaces," American Society of Mechanical Engineers Paper No. 77-WA/SOL-1, 1978.

18. E. R. G. Eckert and R. M. Drake, Jr., Analysis of Heat and Mass Transfer, (New York: McGraw-Hill Book Co., 1972), pp. 522-540.

19. F. W. Sears and G. L. Salinger, Thermodynamics, Kinetic Theory, and Statistical Thermodynamics, (3rd ed; Reading, MA: Addison-Wesley Publishing Company, 1975), pp. 42-48.

UNLIMITED RELEASE

INITIAL DISTRIBUTION

UC-62 (170)

U.S. Department of Energy (6)
Forrestal Building
1000 Independence Avenue, S.W.
Washington, D.C. 20585
Attn: H. Coleman
C. Carwile
K. Cherian
C. Mangold
M. Scheve
T. Wilkins

U.S. Department of Energy (2)
P.O. Box 5400
Albuquerque, NM 87115
Attn: G. Pappas
J. Weisiger

U.S. Department of Energy (3)
1333 Broadway
Oakland, CA 94612
Attn: R. Hughey
G. Katz
W. Lambert

New Mexico State University (10)
Department of Mechanical Engineering
Las Cruces, NM 88001
Attn: G. P. Mulholland (5)
D. B. Wilson
T. R. Mancini
L. Mathews
D. R. Smith
R. Hills

University of California
Department of Electrical and Computer Engineering
Davis, CA 95616
Attn: M. Soderstrand

University of Houston
Solar Energy Laboratory
4800 Calhoun
Houston, TX 77704
Attn: A. Hildebrandt

Aerospace Corporation
2350 El Segundo Blvd.
El Segundo, CA 90245
Attn: P. Munjal

ARCO Power Systems (2)
7061 S. University, Suite 300
Littleton, CO 80122
Attn: F. Blake
D. Gorman

Arizona Public Service Company (2)
P.O. Box 21666
Phoenix, AZ 85036
Attn: J. McGuirk
E. Weber

Babcock and Wilcox (3)
91 Stirling Avenue
Barberton, OH 44203
Attn: G. Grant
I. Hicks
D. Smith

Badger Energy, Inc.
One Broadway
Cambridge, MA 02142
Attn: C. A. Bolthrunis

Bechtel Group, Inc.
P.O. Box 3965
San Francisco, CA 94119
Attn: G. W. Braun
J. Darnell
P. DeLaquil III

Black and Veatch Consulting Enginners (2)
P.O. Box 8405
Kansas City, MO 64114
Attn: J. C. Grosskreutz
J. E. Harder

Boeing Engineering and Construction Company
P.O. Box 3707
Seattle, WA 98124
Attn: R. B. Gillette

Burns & McDonnell
P.O. Box 173
Kansas City, MO 64141
Attn: M. Soderstrum

California Energy Commission
1111 Howe Avenue, MS-70
Sacramento, CA 95825
Attn: D. Pierson

Combustion Engineering, Inc.
1000 Prospect Hill Road
Windsor, CT 06095
Attn: C. R. Buzzuto

DFVLR
Apartado 19, Tabernas
Almeria, Spain
Attn: M. Becker

El Paso Electric Company
P.O. Box 982
El Paso, TX 79946
Attn: J. E. Brown

Electric Power Research Institute
P.O. Box 10412
Palo Alto, CA 94303
Attn: E. DeMeo

Foster Wheeler Development Co. (2)
12 Peach Tree Hill Road
Livingston, NJ 07039
Attn: S. F. Wu
R. Zoschak

Georgia Institute of Technology
Atlanta, GA 30332
Attn: C. T. Brown

Gibbs and Hill, Inc.
393 Seventh Avenue
New York, NY 10001
Attn: J. J. Jimenez

Institute of Gas Technology
Suite 218
1825 K. Street, N.W.
Washington, DC 20036

Martin Marietta (2)
P.O. Box 179, L#0450
Denver, CO 80201
Attn: T. Heaton
T. Tracey

McDonnell Douglas (2)
5301 Bolsa Avenue
Huntington Beach, CA 92647
Attn: C. Finch
L. W. Glover

Olin Chemicals Group
P.O. Box 2896
Lake Charles, LA 70624
Attn: J. Morgan

Olin Chemicals Group (2)
120 Long Ridge Road
Stamford, CT 06904
Attn: F. N. Christopher
L. C. Fiorucci

Pacific Gas and Electric Company
3400 Crow Canyon Road
San Ramon, CA 94526
Attn: C. Weinberg

Pacific Northwest Laboratory (2)
P.O. Box 999
Richland, WA 9932
Attn: B. Johnson
S. Hauser

Public Service Company of New Mexico
P.O. Box 2267
Albuquerque, NM 87103
Attn: A. Akhil

Rockwell International (2)
Energy Systems Group
8900 De Soto Avenue
Canoga Park, CA 91304
Attn: T. Springer
A. Z. Ullman

Solar Energy Industries Association
1156 15th Street, NW
Suite 520
Washington, DC 20005
Attn: C. LaPorta

Solar Energy Research Institute (3)
1617 Cole Boulevard
Golden, CO 80401
Attn: J. Anderson
M. Murphy
L. Shannon

Southern California Edison (3)
P.O. Box 800
Rosemead, CA 92807
Attn: J. N. Reeves
P. Skvarna
R. S. Williamson

Stearns-Roger
P.O. Box 5888
Denver, CO 80217
Attn: W. R. Lang

Stone and Webster Engineering Corporation
P.O. Box 1214
Boston, MA 02107
Attn: R. W. Kuhr

White Sands Missile Range
Material Test & Evaluation Directorate
Nuclear Effects Division
WSMR, NM 88002
Attn: R. M. Marshall

Westinghouse Electric Corporation
Advanced Energy Systems Division
P.O. Box 10864
Pittsburgh, PA 15236
Attn: J. R. Maxwell

Sandia National Laboratories

1824 R. B. Pettit
1824 A. R. Mahoney
6200 V. Dugan
6220 D. G. Schueler
6222 J. V. Otts
6222 R. D. Aden
6222 H. H. Baxter
6222 C. P. Cameron
6222 W. A. Couch
6222 R. M. Edgar (3)
6222 J. T. Holmes
6222 C. W. Mathews
6222 S. L. Murphy
6222 M. A. Quintana
6222 J. M. Stomp
6222 J. W. Strachan
6222 R. Ferreri
6222 P. Gerrish
6222 G. Lang
6222 C. Tappan
6222 S. Saloff
6222 V. Dudley
6222 W. Einhorn
6222 L. Nelson
6222 L. Evans
6222 C. Maxwell
6400 A. W. Snyder
6420 J. V. Walker
6420 M. Watkins
6421 T. R. Schmidt

6422 D. A. Powers
6423 P. S. Pickard
6425 W. J. Camp
6427 M. Berman
6427 B. W. Marshall, Jr. (20)
8000 R. S. Claassen
8000A C. S. Selvage
8100 D. M. Olson
8200 A. N. Blackwell
8300 D. L. Hartley
8124 C. Hartwig
8125 M. E. John
8132 J. Kraabel
8220 R. L. Rinne
8410 R. A. Baroody
8420 A. G. Schuknecht
8440 H. Hanser
8450 J. B. Wright
8452 A. C. Skinrood
8452 D. N. Tanner
8453 J. C. Swearengen
8454 J. B. Woodard
8460 J. F. Barham
3141 Technical Library Processes Division (5)
3141 C. M. Ostrander (5)
3151 W. L. Garner

Org.	Bldg.	Name	Rec'd by	Org.	Bldg.	Name	Rec'd by
6222		Maxwell					

Sandia National Laboratories